Semiconductor Film Cherenkov Lasers

Final Progress Report

John E. Walsh

December 28, 1994

U.S. Army Research Office
Contract No. DAAL03-91-G-0189

Dartmouth College
Hanover, N.H. 03755

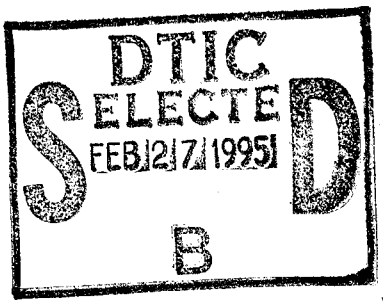

Approved for Public Release:
Distribution Unlimited

Semiconductor Film Cherenkov Lasers

Final Progress Report

John E. Walsh

December 28, 1994

U.S. Army Research Office
Contract No. DAAL03-91-G-0189

Dartmouth College
Hanover, N.H. 03755

Approved for Public Release:
Distribution Unlimited

REPORT DOCUMENTATION PAGE

Form Approved
OMB No. 0704-0188

1. AGENCY USE ONLY (Leave blank)	2. REPORT DATE	3. REPORT TYPE AND DATES COVERED
	28 Dec. 1994	FINAL: 06-01-91 - 05-31-94

4. TITLE AND SUBTITLE

Semiconductor Film Cherenkov Lasers

5. FUNDING NUMBERS

DAAL03-91-G-0189

28531-PH

6. AUTHOR(S)

John E. Walsh

7. PERFORMING ORGANIZATION NAME(S) AND ADDRESS(ES)

Dartmouth College
Department of Physics & Astronomy
6127 Wilder Laboratory
Hanover, N.H. 03755-3528

8. PERFORMING ORGANIZATION REPORT NUMBER

9. SPONSORING/MONITORING AGENCY NAME(S) AND ADDRESS(ES)

U. S. Army Research Office
P. O. Box 12211
Research Triangle Park, NC 27709-2211

10. SPONSORING/MONITORING AGENCY REPORT NUMBER

11. SUPPLEMENTARY NOTES

The view, opinions and/or findings contained in this report are those of the author(s) and should not be construed as an official Department of the Army position, policy, or decision, unless so designated by other documentation.

12a. DISTRIBUTION/AVAILABILITY STATEMENT

Approved for public release; distribution unlimited.

12b. DISTRIBUTION CODE

13. ABSTRACT *(Maximum 200 words)*

The technical achievements for the project "Semiconductor Film Cherenkov Lasers" are summarized. Described in the fourteen appendices are the operation of a sapphire Cherenkov laser and various grating-coupled oscillators. These coherent radiation sources were operated over the spectral range extending from 3 mm down to 400 μm. The utility of various types of open, multi-grating resonators and mode-locked operation were also demonstrated. In addition to these experiments, which were carried out with a 10-100 kV pulse generator, a low-energy (3-3.6 MeV) Van de Graaff generator and a low-energy RF linac (2.8 MeV) were used to investigate the properties of continuum incoherent Smith-Purcell radiation. It was shown that levels of intensity comparable to the infrared beam lines on a synchrotron could be obtained and thus that grating-coupled sources are potentially an important new source for Fourier transform spectroscopy. Finally, a scanning electron microscope was adapted for investigating μ-electron-beam-driven far-infrared sources. At the close of the project, spontaneous emission over the 288-800 μm band had been observed. Intensity levels were in accord with expectations based on theory. One or more of the Appendices address these topics in detail.

14. SUBJECT TERMS Cherenkov Lasers; Grating-coupled sources; Micro-electronic submillimeter source

15. NUMBER OF PAGES 62

16. PRICE CODE

17. SECURITY CLASSIFICATION OF REPORT	18. SECURITY CLASSIFICATION OF THIS PAGE	19. SECURITY CLASSIFICATION OF ABSTRACT	20. LIMITATION OF ABSTRACT
UNCLASSIFIED	UNCLASSIFIED	UNCLASSIFIED	UL

Table of Contents

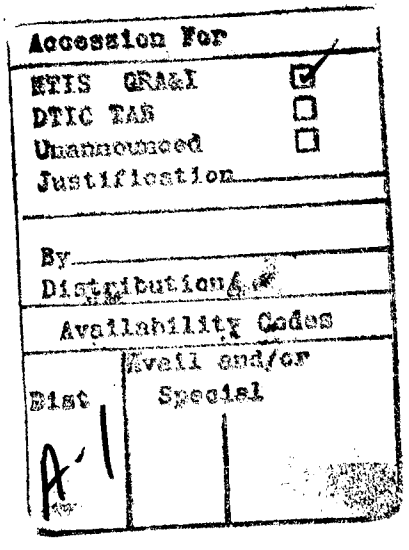

1. Summary of the Most Important Results

Introduction

The goal of the project was to explore techniques which could form the basis of one or more classes of micro-free-electron lasers. Emphasis in particular was on sources which will operate in the submillimeter and far-infrared regions of the spectrum. This is a spectral regime which has a comparative dearth of tunable coherent radiators, but many interesting scientific questions remain and there a range of technical applications.

The terms "compact" or "micro" are qualitative and they must be defined in context with existing devices. Two definitions are employed in this work. First, a device was regraded as "compact" if it used either a low-energy, radio-frequency or a small electrostatic accelerator (< 5 - 10 MeV). These devices are compact in the sense that they easily fit in a laboratory and the shielding requirements are modest.

Second, there are a range of applications where still smaller devices are either preferred or required. The aim in this second category was to develop sources which use electron beams with energies at least below 100 keV. If possible, energies as much as one order of magnitude smaller than this limit are preferred. At the lower end of this range the power supply art has reached a point where sources capable or producing 10's of kV at Watt levels of total power, are readily available. The packages can be small (a few 10's of cm^3) and light-weight (kg.'s).

Proof-of-principle low-energy experiments were conducted with a modified scanning electron microscope. This beam generator was itself "small". In addition, the beam parameters (< 40 kV, < 100 mA) were compatible with newer versions of ultra-compact high-voltage power supplies. Thus, in the final analysis, designs for sources based on this approach would be competititve in size and power consumption with solid state devices.

The primary results of the project have been published in the refereed literature and these publications are included as appendices to this report. In addition, 5 doctoral theses and 3 senior honors theses were completed with the aid of partial support from the project. The theses are listed as a bibliography in Section 5 of this report. What follows in the remainder of this introduction is a summary of the principal results and a guide to the published work.

Cherenkov Radiators

The first effort on the project was expended on attempts to develop micro-scale thin film Cherenkov free-electron lasers. In order to exploit this effect and yet use comparatively low energy electron beams, materials with high index of refraction were needed. Semiconductors were chosen for the first investigations. Since their indices of refraction in the desired spectral range are typically 3 - 4 the threshold velocity for Cherenkov radiation can be achieved with beam voltages below 30 kV. An extensive series of tests were carried out using semiconductor film resonators, but Cherenkov laser action was not achieved. It was possible to produce easily observable amounts of radiation at the band gap energy of the material, but it appears that even a very small amount of intercepted beam changes the conductivity of the film by an amount that is sufficient to quench a long-wavelength infrared oscillation. Enhanced conductivity is not a problem with insulating crystals such as fused quartz and boron nitride, but these low-index materials require relatively high energy (>100 KeV) beams.

In order to complete the investigation of high-index materials for Cherenkov devices, a series of experiments were carried out with free-standing sapphire resonators. Sapphire, with an index of about 3, has a voltage threshold below 20 kV. Emily Fisch developed a "sapphire Cherenkov laser". This work is reported in her doctoral thesis, *The sapphire Cherenkov laser,* defended in September, 1991, and in the two publications *Operation of the sapphire Cherenkov laser* and *Geometric*

approach to wavelength tuning of the Cherenkov free-electron laser. The journal publications are included as Technical Appendices 10 and 12 of this report.

Gratings

In order to circumvent the problem of voltage threshold and dielectric charging (a problem in cw operation), attention was shifted to metal diffraction gratings. The operating wavelengths of a grating-coupled device is determined by the beam velocity, the grating period, and the angle of emission from the grating surface. Two groups of experiments were carried out with low-energy (< 100 keV) beams and additional experiments were also carried out with a 3 - 3.6 MeV Van de Graaff generator and with a 2.8 MeV radio-frequency "injector" linac.

The beam and radiation research group at Dartmouth has had experience with grating-coupled radiators during earlier projects. Sources termed "planar orotrons" and "planar-grating klystrons" were investigated during the 1984-1990 time period. Originally the work was focussed on millimeter-wavelength operation but in the case of the present project, emphasis was shifted to the challenge of achieving oscillation at submillimeter wavelengths. E. Price developed a submillimeter - far-infrared resonator which was comprised of a narrow strip-grating-loaded cylindrical-section-mirror terminated parallel plate waveguide. The structure was generally similar to the ones used in the planar orotron; however, triangular and blazed gratings were used in place of the rectangular profile gratings which had been used in the earlier experiments. Operation over the range extending from 100 GHz (3 mm) to 750 GHz (400 μm) was achieved. At the longer wavelength limit, power levels in the 10's - 100's of W range were obtained and at the short end, W-level powers were observed.

The beam used in this work was formed using a pulse-transformer-driven thermionic electron gun that was constructed originally for Cherenkov maser

experiments, and the transverse dimension of this beam (mm's) was poorly matched to the resonator which at short wavelengths, supported modes with submillimeter evanescence scales. Thus, the efficiency was low, always < 1% and at the shortest wavelengths, it fell between 0.01 and 0.1%. However, it is important to recognize that this is not an intrinsic limit but simply a question of electron beam optics. This point will be discussed further when the work which employed micro beams is summarized. Price's work is described in his doctoral thesis, *Operation of a Smith-Purcell free-electron laser at submillimeter wavelengths* and in the publication *Operation of the grating-coupled oscillator at submillimeter/ far-infrared wavelengths* (Appendix No. 13).

J. Killoran extended the work of Price. Killoran explored a class of open resonators formed by replacing the top plate of the waveguide with a second grating and removing the end mirrors. These modifications to the resonator geometry are an important evolutionary step in developing a short-wavelength device. It separates the beam transport and mode containment functions. Resonators formed with two gratings may also have high unloaded quality factors and they present an number of intriguing options for designing output couplers (higher-order diffraction, etc.). Killoran worked over the same general spectral range as Price, and a summary of his results are to be found in his doctoral thesis, *Investigations of a Smith-Purcell free-electron laser at submillimeter wavelengths* and in the journal article *Millimeter wavelength radiation source using a dual grating resonator* (Appendix No. 8).

The mode-locking experiments were carried out by F. Hacker who worked in the 5 - 8 mm wavelength range,. However, in spite of the comparatively long wavelength they, too, are an important step forward for short-wavelength source development. In principal, just as is the case in a conventional laser, mode locking provides a means of producing short pulses if high peak power beginning with what

is nominally a cw source. At the present moment, Hacker's results are available only in his thesis; a summary of the work is being prepared for publication.

Micron-Scale Beam Generation

All of the experiments described in the preceding section were carried out using the pulse-transformer-based beam generator which has been described in many of the early publications (see Felch *et al., Cerenkov Radiation in Dielectric-Lined Waveguides,* Appl. Phys. Lett. **38(8)**, 601 (1981).

This has been a very serviceable beam generator but as already mentioned, the physical size of the beam is not well suited for work at lower-mm and shorter wavelengths. In order to remedy this problem and to otherwise explore the beam parameter space region which would lead ultimately to micro-scale devices, experiments were carried out with a beam formed in an electron microscope. An AMR-1000 scanning electron microscope (SEM) was acquired and modified in such a way as to allow operation at somewhat higher voltage and current than anticipated in the original design of the instrument ($V \leq 50$ kV *vs.* 30 kV and I ~ 10's of μA *vs.* < μA). The SEM was otherwise left intact, and in fact it still operates as an SEM.

In a final design of a device the microscope would of course be replaced by a much smaller electron optical system, but during the exploratory phase of the project the ability to focus and position the electron beam with great precision is an extraordinary advantage. The beam's transverse size (10-20 μm or smaller, if desired) is compatible with operation anywhere in the far-infrared spectral region. The gratings can be mounted on the microscope stage and this gives an important degree of freedom in positioning the resonator with respect to the beam axis. As the project drew to a close, the first observations of spontaneous emission had been completed. Radiation that was tunable over the range from 288 μm to a bit above 800 μm had been produced an the intensity levels were consistent with expectations

based on theory. The the latter point is extremely important in that it provides confidence in the set of assumptions that also form the basis of a gain calculation. On the strength of these results, we can conclude that a coherent, tunable, grating-coupled oscillator which employs truly compact e-beam technology, is a realistic objective.

The results of the experiments with the SEM have not yet been submitted for publication, but the essential details are to be found in *A far-infrared Smith-Purcell micro-radiator,* M. Goldstein's doctoral thesis. An abstract, *Smith-Purcell experiments with a scanning electron microscope* (for a presentation which was made during the APS Division of Plasma Physics Meeting) is attached as Appendix 4. Also included (Appendix 1) is the preprint of a manuscript by Tang *et al., Micro free-electron lasers.* This work will be published in Nuclear Instruments and Methods. Among other topics it addresses the challenges and potential value of integrating modern low-voltage, high-current-density, field emission cathodes with micro-resonators.

Van de Graaff and Radio-Frequency Accelerators

In the first part of this summary experiments with relativistic electron beams were mentioned and some of the main results from this work are summarized in Appendices 2 and 14. The work carried out in collaboration with colleagues at Oxford University used a 3-3.6 MeV Van de Graaff accelerator and in these experiments, tuning from a wavelength of approximately 280 μm to beyond a mm was demonstrated. The power levels from even the rather poorly-collimated 100 mA beam were comparable to that available from a typical infrared beam line on a synchrotron (at comparable wavelengths). The predicted and measured wavelengths are in excellent agreement and this, together with the intriguing levels of intensity from even the spontaneous emission, suggest that radiation from

gratings driven by relativistic beams may be a very practical source of infrared radiation. In order to explore this concept further, the interaction chamber used in the Oxford experiments was moved to Brookhaven National Laboratory and mounted on the injector section of the ATF accelerator. The first results from the Brookhaven collaboration are summarized in the Appendix No. 2.

Theory

Although gratings have been in use for more than two centuries and detailed experimental and theoretical investigations have been conducted for more than a century, they remain a subject for interesting research. In the case of the work on this project, it was necessary to develop a theory which could describe the way in which the grating profile would affect emission efficiency. The method developed by van den Berg (Ref. [6] in Appendix No. 2) was adapted for this purpose and descriptions of what has been accomplished can be found in the Killoran and Goldstein theses. A conceptually simple approach to calculating the emission intensity is also described in Appendix 9. In this note the separability of the emission calculation into phase space related factors and actors which depend on the grating profile was demonstrated. This instructive concept is still under active investigation.

Conclusion

The work summarized in this introduction is described in more detail in the appendices which follow. Additional detail may be found in the theses listed in Section 5.

2. List of Technical Appendices

1. *Micro Free Electron Lasers,* C.M. Tang, M. Goldstein, T.A. Swyden and J.E. Walsh, to be published in Nuclear Instruments and Methods, 1995.

2. *Forward Enhancement of Smith-Purcell Radiation from Relativistic Electrons,* K. J. Woods, J.E. Walsh, R.E. Stoner, H.G. Kirk and R.C. Fernow, to be submitted to Applied Physics Letters.

3. *Smith-Purcell Radiation in the Relativistic Limit,* Abstract presented at the International Conference on Free-Electron Lasers, Stanford, Ca., August 1994.

4. *Smith-Purcell Experiments with a Scanning Electron Microscope,* M. Goldstein and J.E. Walsh, Abstract presented at the 36th Annual Meeting, APS Division of Plasma Physics, November 1994.

5. *Forward Peaking of Relativistic Electron-Beam-Generated Smith-Purcell Radiation,* K.J. Woods, R.E. Stoner, R. Fernow, H.G. Kirk and J.E. Walsh, *idem.*

6. *Smith-Purcell Radiation in the Relativistic Limit,* J.E. Walsh, S.G. Yeager and K.J. Woods, *idem.*

7. *Smith-Purcell Radiation in the Relativistic Electron Beam Limit,* J.E. Walsh, K. Woods, R.E. Stoner, R. Fernow, H.G. Kirk and X. Wang, Abstract presented at the Spring Meeting of the American Physical Society, April 1994.

8. *A Millimeter Wavelength Radiation Source Using a Dual Grating Resonator, J.H. Killoran,* F.L. Hacker and J.E. Walsh, IEEE Trans. Plas.Sci. **22**(5), October 1994.

9. *Intensity of Smith-Purcell Radiation in the Relativistic Regime,* J.E. Walsh, K.J. Woods and S.G. Yeager, Nucl.Instrum.Meth. A **341,** 277 (1994).

10. *Geometric Approach to Wavelength Tuning of the Cherenkov Free-Electron Laser,* E.E. Fisch and J.E. Walsh, Opt.Lett. **17**(11), 813 (1994).

11. *First Observation of Smith-Purcell Radiation from Relativistic Electrons,* G. Doucas, J.H. Mulvey, M. Omori, J.E. Walsh and M.F. Kimmitt, Phys.Rev.Lett. **69**(12), 1761 (1992).

12. *Operation of the Sapphire Cherenkov Laser,* E.E. Fisch and J.E. Walsh, Appl. Phys.Lett. **60**(11), 1298 (1992).

13. *Operation of the Grating-Coupled Oscillator at Submillimeter/Far-Infrared Wavelengths,* E.J. Price and J.E. Walsh, Appl.Phys.Lett. **61**(3), 252 (1992).

14. *First Observation of Smith-Purcell Radiation from Relativistic Electrons,* G. Doucas, J.H. Mulvey, M. Omori, J.E. Walsh and M.F. Kimmitt, Abstract presented at the European Particle Accelerator Conference, Geneva, Switzerland, April 1992.

MICRO FREE ELECTRON LASERS

C. M. Tang,[a] M. Goldstein,[b] T. A. Swyden[c] and J. E. Walsh[b]

[a] Permanent address: Plasma Physics Division, Naval Research Laboratory, Washington, DC 20375-5346

Current address: National Institute of Standards and Technology, Gaithersburg, MD 20899

Tel: (301) 975-4272 - Fax: (301) 975-3038

[b] Dartmouth College, Hanover, NH 03755

[c] FM Technologies, Inc., Fairfax, VA 22032

Abstract

The electron optical properties of microscopic gated field emitter arrays (FEA) are an ideal match to the electron beam requirements of micro free electron lasers. Projected performance characteristics of the beam generators based on the FEA principle are reviewed and results from recent experiments with a single micro beam filament are summarized. The latter are shown to support the claim that micro free electron lasers based on either the Čerenkov or Smith-Purcell interaction mechanism are a practical possibility.

(Submitted for the Proceedings of the 1994 Conference on Free-Electron Lasers in Stanford, CA; to be published in Nuclear Instruments and Methods, 1995).

1. Introduction

Spectroscopic and other commercial applications of lasers typically require systems with low to moderate power, compact size and inexpensive cost. Various free-electron laser mechanisms, particularly Smith-Purcell or Čerenkov devices, driven by micro-electron beams[1-5] are interesting in those contexts. A potential source for the beam is the gated field-emitter array, which has high current density and low emittance. In section 2, we present computer simulations of a simple method of producing collimated sheet beams from gated field-emitters using planar lens fabricated along with the field emitters on the same substrate. The good beam quality of these gated field-emitters imply that tunable infrared oscillators in the IR from tens to hundreds of μm are feasible. In a series of proof of principle experiments spontaneous emission from a Smith-Purcell device has been obtained. Scaling of the radiation wavelength (288μm – 803μm) and the total emitted intensity are in accord with theory.

2. Field-Emitter Technology and Beam Collimation

The generation of short wavelength radiation in a compact size requires good beam collimation and small beam dimensions, i.e., good emittance. Large growth rates for coherent radiation require high current density, i.e., high beam brightness. A compact electron source with the required properties is the gated field-emitter array (FEA). Electrons beams from FEAs can be cw or pulsed. Since FEAs comes in a wide variety of configurations, only a few examples will be given below.

Experimental results pertinent to the FEL is summarized. For emitter tips with large radii of curvature, currents up to 200 μA for single tip have been reported by SRI[6] and even higher currents have been measured in 10^{-6} Torr of hydrogen by Philips Research Laboratory.[7] Field-emitter arrays with submicron gate opening diameters and sharp tips have been fabricated by SRI[6] and MIT/Lincoln Laboratory.[8] SRI utilized focused ion beams to fabricated arrays with gate opening diameters of 0.3 μm, and tip-to-tip separation of 0.5 μm. These tips emitted on average 3 μA per tip at a gate voltage of 45 V. Lincoln Laboratory utilized holographic methods

to fabricate FEAs with gate opening diameters of 0.16 μm and tip-to-tip separation of 0.32 μm. They measured on average 1.0 μA per tip at a gate voltage around 30 - 35 V.[9] Refinements in FEA processing are continuing to improve the current per tip, lower gate voltages for electron emission, increase current density, improve lifetime, etc.

The emittance associated with each cone-emitter is small because electron emission occurs only from their tip which has a radius of curvature typically much less than 100 Å. Using EGUN2[10] to estimate the RMS normalized emittance associated with emitters, we find values typically on the order of a few 10^{-4} π–mm–mrad. A simulation example will be given below.

Despite the low emittance, electron emission patterns from FEA tips have large angular spreads. It is, however, possible to apply focusing lenses to collimate the beams. There are various approaches to beam focusing, but we will limit discussions to two types of electrostatic lens: the thin overlapping lens and a planar lens for gated cone emitters.

A schematic of a generic thin overlapping lens is shown in Fig. 1. For the thin lens to be effective, the lens opening has to be self-aligned with the gate opening, and the distance of the lens from the gate should be much less than the gate opening diameter. Computer simulations indicate the lens voltage will be comparable to tip voltage for best collimation.[11–13] The overlapping thin lens, however, is difficult to fabricate. Recently, a self-aligned thin lens and gate geometry was successfully made[14] and beam focusing was demonstrated experimentally. The experimental results agree qualitatively with the computer simulations. A potential disadvantage of the thin lens is an experimentally observed reduction in the output current with increased focusing, because of a lowering of the field at the emitter tip due to the proximity of the low lens voltage and possibly because of charging of the insulator between the gate and the lens.

In contrast, the coplanar lens and nearly coplanar lens,[15–21] shown in Figs. 2a and 2b, respectively, are very simple to fabricate. For the planar lens to be effective, the lens electrodes must extend over a wide lateral area around the gate

electrode. Focusing occurs in a substantial region above the gate surface, providing beam collimation for an effectively larger percentage of the outer beam electrons. Since the lens electrode is now some distance from the tip, the field reduction at the tip by the lens is not expected to be significant. Planar lenses have previously been used for thermionic cathodes. For field-emitters, the integration of the lens with the emitters on the same substrate simplifies alignment and implementation. Planar lens focusing for FEAs has been demonstrated experimentally.[18–19]

A self-consistent EGUN2 simulation of a gated field-emitter with a planar lens is shown in Fig. 3. RMS normalized emittance is calculated by EGUN2 to be 2.1×10^{-4} π–mm–mrad in the cylindrical geometry. The parameters used in this simulation are: gate voltage of 20 V, gate diameter of 0.16 μm, radius of curvature of the tip of 50 Å, lens voltage of -15 V, anode voltage of 51.25 V located at a distance of 5 μm from the gate and current of 1 μA/tip. The electron beam radius at 10 keV is about 3 μm. The emittance would vary somewhat with slightly different sets of parameters, but is expected to remain around the same order of magnitude.

Next, we show that integrated planar lenses may provide a simple method of producing collimated sheet beams from field-emitters. We consider FEAs with small gate diameters densely packed along a line yielding a current of 10 μA/μm at a gate voltage of 50 V. The emitters and substrate are at ground. We assume a linear gate electrode 1 μm wide separated on either side from the planar lens by a 0.5 μm gap. [Fabrication of a 1 μm gate width using current ion beam systems is difficult, but there is no inherent problems in making self-aligned 1 μm wide gates with submicron gate diameters.] Lacking a three-dimensional simulation capability for field-emitters, emission from the tip of the cone emitter into a linear geometry that is not rotationally symmetric, cannot be modeled exactly. The following EGUN2 simulations assumed electron emission in the (x,z) plane from a point source, with emission angles restricted to $\pm$ 50° and each electron trajectory spaced 5° apart.

For an accelerating field of 5.0 V/μm, we show beam collimation by a planar lens at -15 V in Fig. 4. Electrons initially emitted within $\pm$25° are confined in a narrow beam, while the outer rays can be eliminated by aperture. A very low

current when space charge is negligible, the collimated beam spot sizes is about 10 μm at 40 keV without any additional focusing. For high current densities such as 10 μA/μm, when space charge becomes important, it may be better not to focus the beam so tightly at low voltage. Additional focusing may be needed for space charge dominated beams.

Wider gate strips allow larger gate diameters that can be fabricated using a wide variety of available methods. Larger gate diameters require higher gate voltages for emission. In the next example, we assume a gate voltage of 100 V, with the emitter and the substrate at ground, and a gate electrode 4 μm wide separated on either side from the planar lens by a 1.0 μm gap. Again, we assume an averaged line current greater than 10 μA/μm. As before, EGUN2 simulated electron emission in the (x,z) plane from a point source with emission angles restricted to $\pm$ 50° and each electron trajectory separated by 5°. We show beam collimation by a planar lens at -35 V in an accelerating field of 5.0 V/μm in Fig. 5.

3. Smith-Purcell Experiments with a Micro Electron Beam

The beams of the type described in section 3 might be used to generate radiation from a diffraction grating. When an electron beam is passed over the surface of a metal grating Smith-Purcell radiation is emitted.[22] If the beam travels perpendicular to grooves of spacing, D, the wavelength spectrum is

$$\lambda = \frac{D}{|m|}\left(\frac{1}{\beta} - \sin(\theta_m)\right),$$

where $\beta \equiv v_b/c$ is the electron velocity divided by the speed of light. The angle, θ_m, is measured between the grating normal and the propagating direction of a wave with spectral order $m = -1, -2, -3, \ldots$. In order to couple effectively the beam must be located a distance (d) from the surface which obeys the constraint, $d \lesssim \lambda\beta\gamma/2\pi$, where $\gamma \equiv (1-\beta^2)^{-1/2}$.

At Dartmouth College, experiments have generated Smith-Purcell radiation[1] with wavelengths ranging from 288 to 803 μm. A 178μm period diffraction grating generated, $(1.0 \pm 0.2) \times 10^{-8}$ watts/Str., at 476μm in a 40μm bandwidth. The

emitting surface area was 6×10^{-8} m^2. Thus, a basic radiance of approximately 0.17 watts/(Str. m^2) was produced.

A scanning electron microscope was used as an electron beam source in these experiments. The beam typically had a radius that varied from 3 to 30 μm, carried a 50 μA current, and had an energy of 30 - 40 kilovolts and with a normalized emittance of $\epsilon_n \approx 10^{-2}$ π–mm–mrad. The beam in these experiments was formed by a tungsten cathode, focused with magnetic lenses and scraped with platinum apertures. The general beam parameters were inferior to what could be generated with an FEA. A linear array could be used in a number of feedback geometries to form an oscillator.

4. Summary

Good agreement between theory and experiment for Smith-Purcell radiation was observed for micro gratings with beam from electron microscope. Electron beams from FEAs have demonstrated high current density and is predicted to have small emittance. Good beam collimation would be possible. Planar lens, simple to fabricate and easy to implement, may provide useful collimated beams. When the small emittance of the field-emitters is confirmed experimentally for sheet beams, compact, tunable oscillators in the infrared with gratings may be possible down to tens of μm in wavelength.

Acknowledgements

Work supported by ONR and the ARO contract DAAL03-91G-0189.

References

1. Michael Goldstein, Thesis in preparation. Ph.D. Thesis, Dartmouth College, 1994.
2. K. Mima, et al., Nucl. Instrum. and Methods **A331**, 550 (1993).
3. T. Taguchi and K. Mima, Nucl. Instrum. and Methods **A331**, 597 (1993).
4. K. Mima, et al., Nucl. Instrum. and Methods **A341**, ABS 103, 1994.
5. T. Taguchi and K. Mima, Nucl. Instrum. and Methods **A341**, 322, 1994.
6. C. A. Spindt, private communications
7. G. N. A. van Veen, private communications
8. C. O. Bozler, et al., J. Vac. Sci. Technol. **B12**, 629 (1994).
9. M. Hollis, private communications
10. W. B. Herrmannsfeldt, EGUN - An Electron Optics and Gun Design Program, SLAC Report 331 (1988).
11. C. M. Tang, A. C. Ting and T. A. Swyden, "Field-Emission Arrays – A Potentially Bright Source", Nuclear Instrum. and Methods **A318**, 353 (1992).
12. W. B. Herrmannsfeldt, R. Becker, I. Brodie, A. Rosengreen and C. A. Spindt, Nuclear Instrum. and Methods in Phys. Res. **A298**, 39 (1990).
13. R. M. Mobley and J. E. Boers, "Computer Simulation of Micro-Triode Performance", IEEE Trans. on Electron Devices **38**, 2383 (1991).
14. J. Itoh, K. Morikawa, Y. Tohma and S. Kanemaru, Revue "Le Vide, les Couches Minces" – Supplément au No 271 – Mars-Avril 1994, p. 25.
15. C. A. Spindt, "Automatically Focusing Field Emission Electrode", U. S. patent 4,874,981 (1989).
16. T. Leroux and C. Py, "Systéme permettant de maitriser la forme d'un faisceau de particules chargées", French patent 92403558.7 (1992).
17. W. D. Kesling and C. E. Hunt, "Field Emission Device Modeling for Application to Flat Panel Displays", J. Vac. Sci. Techn. **B11**, 518 (1993).
18. C. M. Tang, T. A. Swyden, A. C. Ting, X. F. Liu, L. Yadon, C. T. Sune and G. W. Jones, Technical Digest of the 1993 IEEE Intl. Electronics Devices Meeting, Washington, DC, 5-8 Dec. 1993, pp. 761-764.

19. C. M. Tang, T. A. Swyden and A. C. Ting, "Observation of Focusing from Field-Emitter Arrays", Revue "Le Vide, les Couches Minces" – Supplément au No 271 – Mars-Avril 1994, p. 346.

20. C. E. Holland and C. A. Spindt, "Spindt Cathodes with Coplanar Electrodes", Revue "Le Vide, les Couches Minces" – Supplément au No 271 – Mars-Avril 1994, p. 377.

21. W. D. Kesling and C. E. Hunt, "Beam Focusing for Field Emission Flat Panel Displays", Revue "Le Vide, les Couches Minces" – Supplément au No 271 – Mars-Avril 1994, p. 135.

22. S. J. Smith and E. M. Purcell, Phys. Rev., **92**, 1069 (1953)

Figure Captions

Fig. 1. Schematic of field emitter with thin lens electrode overlapping the gate electrode.

Fig. 2. Schematics of field emitters with planar lens concepts where (a) the lens electrode is coplanar with the gate electrode and (b) the lens electrode is nearly coplanar with the gate electrode.

Fig. 3. Equipotential curves and electron trajectories of a cone emitter simulated by EGUN2 in cylindrical geometry with planar focusing lens.

Fig. 4. Equipotential curves and electron trajectories showing beam collimation with planar lens for gate width of 1 μm and gate voltage of 50 V with the planar lens at -15 V and an accelerating field of 5 V/μm.

Fig. 5. Equipotential curves and electron trajectories showing beam collimation with planar lens for gate width of 4 μm and gate voltage of 100 V with the planar lens at -35 V and an accelerating field of 5 V/μm.

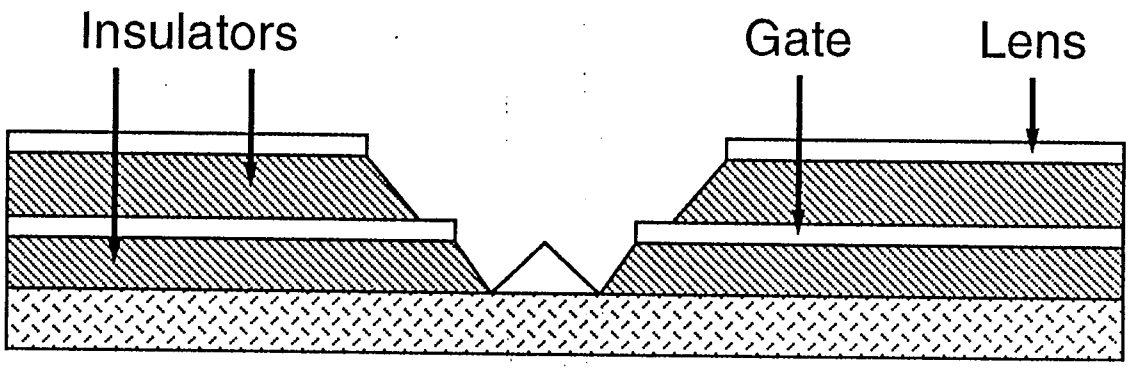

Fig. 1

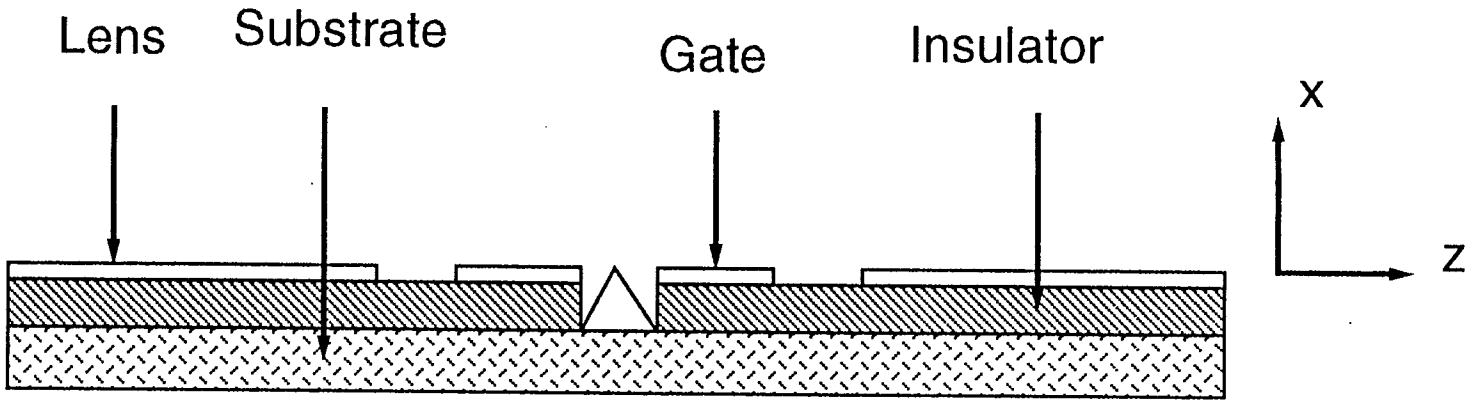

Fig. 2a

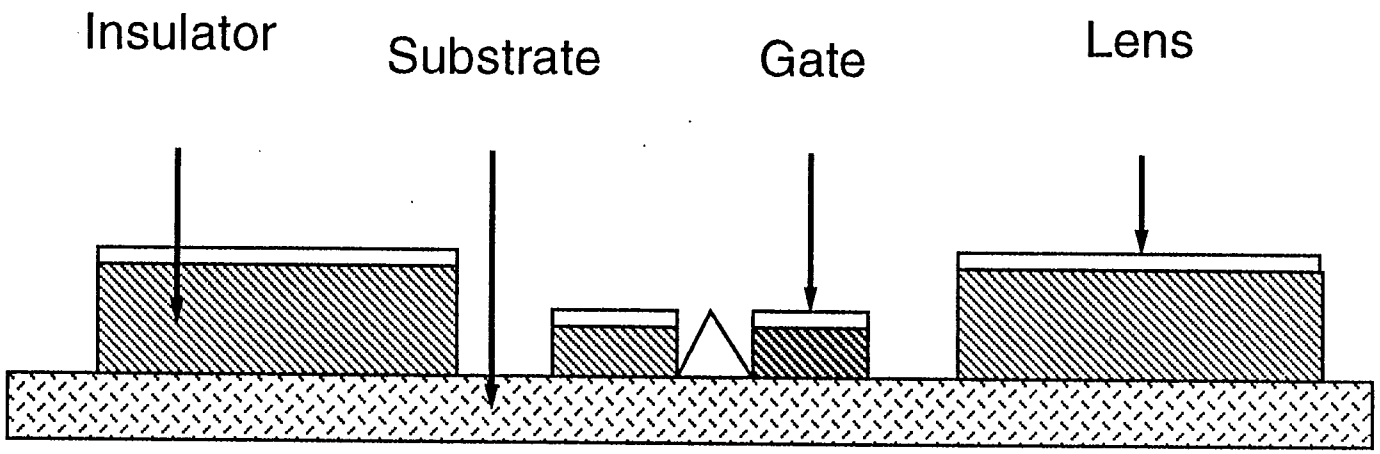

Fig. 2b

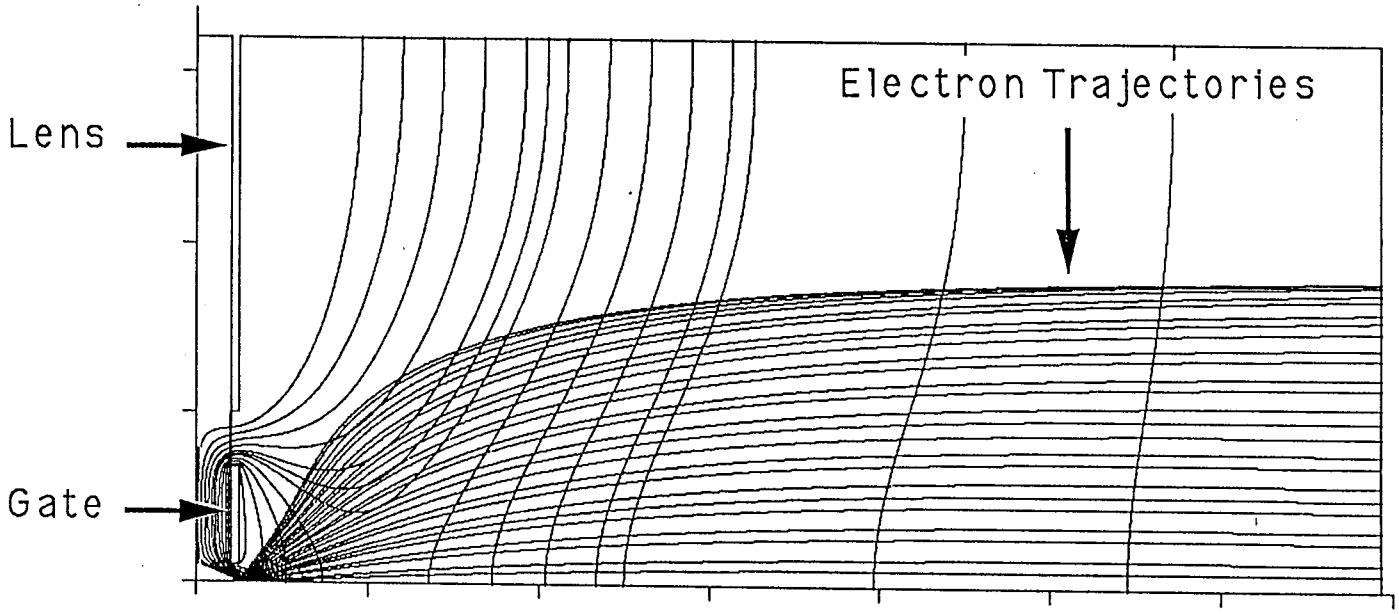

Fig. 3

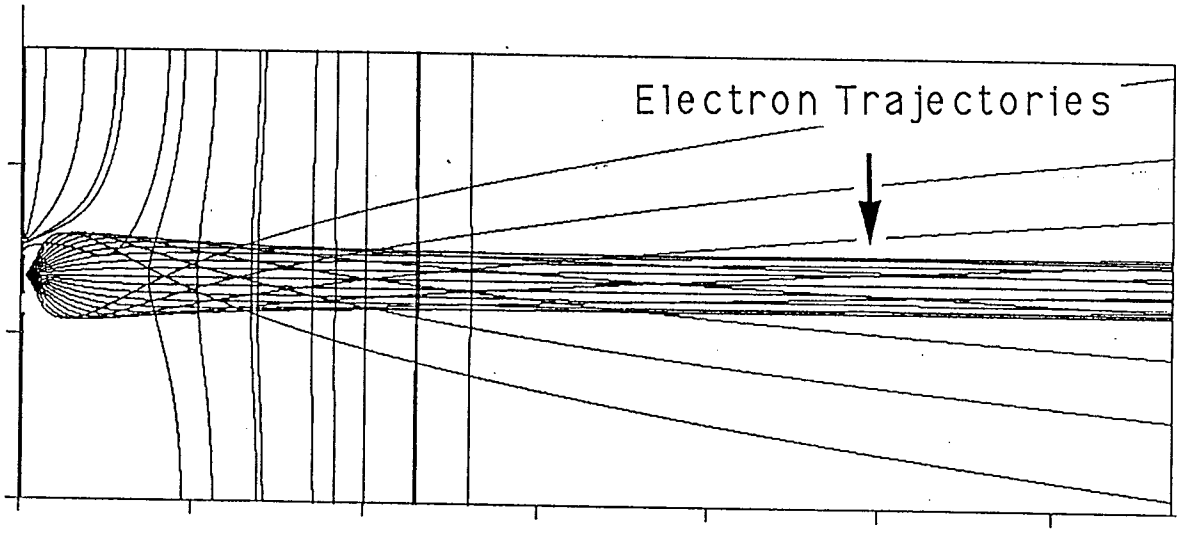

Fig. 4

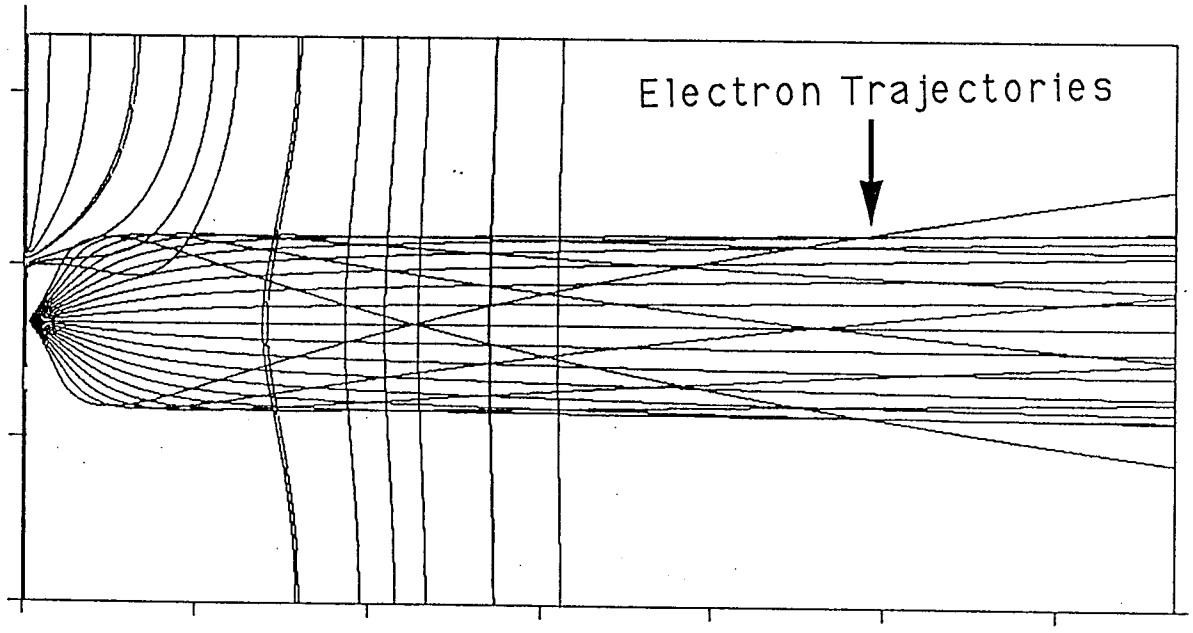

Fig. 5

PREPRINT To be Submitted to Appl. Phys. Lett

Forward Enhancement of Smith-Purcell Radiation from Relativistic Electrons

K. J. Woods and J. E. Walsh
Department of Physics and Astronomy, Dartmouth College, Hanover, NH 03755

R. E. Stoner*
Massachusets Institute of Technology and Research Laboratory of Electronics, Cambridge, MA 02139

H. G. Kirk and R. C. Fernow
Department of Physics, Brookhaven National Laboratory, Upton, NY 11973

(November 3, 1994)

Abstract: The requirements for the generation of enhanced intensity, forward directed Smith-Purcell emission from relativistic electrons are introduced, and the first experimental evidence of this enhancement is presented. In the forward emission the wavelengths radiated are much shorter than the grating period. The experiments were conducted with a 2.8 MeV/c electron beam interacting with a 1 cm period grating. Grating period to wavelength ratios as high as 16 were produced. The measured spectrum indicates that the longitudinal microbunch profile is more rectangular than Gaussian.

PACS numbers: 41.60.-m, 42.79.Dj, 41.75.Ht

The characteristic signature of radiation produced by energetic electrons is a peaking of the emission spectrum along the direction of the electron momentum. Thus it is to be expected on general grounds that Smith-Purcell radiation produced by relativistic electrons will exhibit this structure as well. The first experimental evidence of enhanced forward emission will be presented in this Letter.

In their report on radiation produced by electrons skimming over a diffraction grating, Smith and Purcell [1] introduced the expression

$$\lambda = \frac{l}{|n|}[1/\beta - \cos(\theta)] \qquad (1)$$

which relates wavelength λ, grating period l, the relativistic velocity of the electron β, the emission angle θ, and the diffraction order $|n|$. The emission angle is measured relative to the axis established by the electron's momentum. Equation (1) may be deduced from a Huygens construction, and the expression is valid in either the nonrelativistic or relativistic limit. When $\beta \to 1$, forward emission at $\theta \to 1/\gamma$ (γ being the relativistic factor $1/\sqrt{1-\beta^2}$) will result in wavelengths that are much shorter than the grating period. In order to maintain good coupling between the electron beam and the grating for emission in the forward direction, additional constraints must also be satisfied.

The angular distribution of the power radiated into the n^{th} order from electrons moving over a grating is given by an expression of the general form

$$\frac{dP_n}{d\Omega} = \frac{eIn^2L\beta^3}{2l^2\epsilon_0}\frac{\sin^2(\theta)\cos^2(\phi)}{[1-\beta\cos(\theta)]^3}[1+N_e\mathcal{F}(\alpha)] \times \exp[-\kappa(\theta,\phi)x_0]|R_n(\theta,\phi)|^2 \text{ (W/sr)} \qquad (2)$$

where L is the total grating length, I is the beam current, e is the charge of an electron, N_e is the number of electrons per bunch, and x_0 is the beam height measured from the highest point on the grating surface. An expression similar to Eq. (2) was first published by G. Toraldo di Francia [2] and many general considerations were addressed originally by S. Smith [3]. Equation (2) can also be derived from an elementary model of the emission mechanism [4]. The coordinate system and emission angles θ and ϕ are illustrated in Fig. 1. The wavelength depends only on the polar angle θ, and it should be noted that the solid angle $d\Omega$ and signal bandwidth $d\omega$ are related through Eq. (1). Equation (2) is derived using a delta function beam located at $x = x_0, y = 0$. This is a good approximation for an extended beam if the mean beam height satisfies the condition $x_0 < \beta\gamma\lambda/4\pi$. If this condition is not satisfied an integral over the beam distribution must be substituted for the exponential term.

The function $\mathcal{F}(\alpha)$ is introduced in order to account for possible intensity enhancement due to spatial coherence of the electron bunch. This concept was first discussed during the early development of synchrotrons where it was suggested that it could be a possible mechanism for substantial energy loss [5]. When the longitudinal bunch profile is a Gaussian of length τ then $\mathcal{F}(\alpha)$ is defined as

$$\mathcal{F}(\alpha) = \exp[-(\alpha/2)^2] \qquad (3a)$$

where α is the phase variation relative to the emitted radiation,

$$\alpha = \omega\tau = 2\pi c\tau/\lambda.$$

For a rectangular longitudinal profile the coherence factor becomes

[1]Present address: Smithsonian Astrophysical Observatory Cambridge, MA 02140

$$\mathcal{F}(\alpha) = \left[\frac{\sin(\alpha/2)}{\alpha/2}\right]^2 . \qquad (3b)$$

The angular distribution of the radiation is determined by the two factors $\sin^2(\theta)\cos^2(\phi)/[1-\beta\cos(\theta)]^3$ and $\exp(-\kappa(\theta,\phi)x_0)$. When $\theta \to 1/\gamma$ the dependence of the first of these terms scales as γ^4 near its peak, and the peak narrows in proportion to $1/\gamma^3$. The exponential factor $\exp[-\kappa x_0]$ is a consequence of the fact that the electron beam couples with space harmonic fields on the grating which have a phase velocity less than the speed of light. The evanescent scale is [4]

$$\kappa(\theta,\phi) \doteq \frac{2\omega}{c\beta\gamma}\sqrt{1+[\beta\gamma\sin(\theta)\sin(\phi)]^2} \qquad (4a)$$

or, invoking Eq. (1),

$$\kappa_n = \frac{4\pi|n|\sqrt{1+[\beta\gamma\sin(\theta)\sin(\phi)]^2}}{\gamma[1-\beta\cos(\theta)]l}. \qquad (4b)$$

It follows from Eq. (4b) that in the limit $\theta \to 1/\gamma, \beta \to 1$, the ratio $2\pi x_0/l \simeq 1/\gamma$ must be maintained in order to prevent the exponential factor from cutting off the emission in the forward direction. Thus, the possibly surprising conclusion is reached that l must become quite large in order to maintain good coupling for small emission angles. The emitted wavelength in this limit scales as $\lambda \simeq l/\gamma^2$.

The only factor not yet mentioned is $|R_n(\theta,\phi)|^2$ which, in essence, is a measure of grating efficiency. The concept was first introduced for Smith-Purcell radiation by G. Toraldo di Francia [2], and later van den Berg [6] devised a method for calculating $|R_n(\theta,\phi)|^2$. The van den Berg approach is straightforward but numerically intensive when wavelengths are much shorter than the grating period [7]. Since in this limit the grating period is long in comparison with the emitted wavelength, the grating falls into a class known generally as an echelle [8].

The experimental investigations were conducted on the Accelerator Test Facility (ATF) low-energy beam line at Brookhaven National Laboratory [9]. The beam line consists of a 1-1/2 cell rf photoinjector, profile monitors, momentum slits, a dipole magnet, and focusing quadrupole magnets as well as horizontal and vertical steering magnets. The momentum was tuned to 2.8 MeV/c ($\gamma = 5.6$). The π-mode S-band injector contains a photocathode which was operated in an explosive electron emission mode. Explosive electron emission results from irradiating the cathode with a reduced spot size of the Nd:YAG pulse so that higher laser power densities on the cathode are achieved [10]. The macropulses are typically 20 ns long (57 rf buckets) and contain 2 nC of charge. The repetition rate was 3 Hz. The micropulses are 20 ps long and separated by 350 ps. The measured emittances are on the order of 4 π mm-mrad and peak currents are typically 1-2 A.

The optical collection system is one used previously [11]. As shown in Fig. 2, the Smith-Purcell emission from the grating is reflected off a rotatable plane mirror onto an off-axis parabodial mirror (OAPM). Adjusting the plane mirror angle allows selection of the desired observation angle and therefore the wavelength of the Smith-Purcell radiation. The OAPM focuses the radiation into a light pipe which transports the signal to an optical table. The light pipe was not evacuated.

A beamflag consisting of a phosphor painted aluminum surface was mounted at the front of the grating assembly to allow viewing of the beam profile by a video camera. The video signal was analyzed by a SPIRICON imaging system which allowed a measurement of the beam width, height, and charge distribution. The beam was approximately Gaussian in both directions with a width of 1.2 cm and a thickness normal to the grating of 0.75 mm. The grating height was adjusted so a small fraction of the beam was intercepted by the grating.

The optical collection system was originally designed for viewing emission angles larger than 30 degrees, but for this experiment it was modified to allow collection at smaller angles. The collection system's angular width was approximately 10 degrees and the emission spectrum was centered about the nominal collection angle.

The spectral content of the radiation was analyzed with a Czerny-Turner monochromator and detected with a liquid helium cooled InSb bolometer. The bolometer signal has a very sharp rise and falls off exponentially as the electrons relax to the lattice temperature. The detector/amplifier system responsivity was calibrated at 623 μm with a 5000 K mercury arc lamp. The measured responsivity was 862 V/W for radiation pulse lengths much longer than the response time of the crystal. Since the Smith-Purcell radiation signal was 10 times shorter than the response time of the InSb crystal, the effective power responsivity averaged over the macropulse (20 ns) was $862 \times 20\text{ns}/200\text{ns} = 86.2 \pm 13$ V/W. Signals were averaged over 16 shots on a Tektronix 2431L digital oscilloscope.

An aluminum grating 1.69 cm wide and 17 cm long with a period of 1.0 cm and a blaze angle of 5 degrees was used to investigate forward emission. It was oriented (Fig. 2) such that the electron footprint moves up the shallow slope of the grating. In addition to the grating just described, wavelength measurements were conducted with 30 degree blaze gratings which had periods of 1 mm, 2 mm, and 4 mm and 20 degree blaze gratings with periods of 2 mm and 4 mm. Measured emission angles ranged from 18 to 140 degrees. The measured wavelengths, shown in Fig. 3, are in excellent argeement with the predictions of Eq. (1).

Forward emission observations were made at two mirror settings, 18 and 30 degrees. The 30 degree orientation was chosen because that was the smallest angle for which good collection efficiency could be expected [12]. The 18

degree setting was also examined because it is near the peak of the power spectrum as given by Eq. (2). The spectral content of the two collection settings is shown in Figs. 4 and 5. The detector signal was normalized to the charge measured at the Faraday cup to reduce the effect of shot-to-shot variations in the beam, and a linear relationship between the signal and charge was assumed for this normalization.

In other experiments [13–15] where the long pulse nature of the electron beam makes the limit $\mathcal{F}(\alpha) \to 0$ appropriate, the results indicate that the predicted and measured powers are comparable. Thus Eq. (2) is a reliable predictor of the spontaneous emission from a group of uncorrelated electrons. For our experiments the measured powers were significantly higher than the predictions of Eq. (2) for $\mathcal{F}(\alpha) = 0$. The macropulse average powers measured at the detector were 69.6 μW for a wavelength of 0.623 mm and 78.5 μW for 1.32 mm. For the 18 degree setting only the back half of the grating, or about 8 periods, was collected by the collection system. The power from the entire grating would be a factor of two higher. In the limit $\mathcal{F}(\alpha) = 0$ (no spatial coherence) the emission levels predicted by Eq. (2) for the experimental parameters are 1.2 μW for 0.623 mm and 34 nW for 1.32 mm. The collected solid angles of 0.0054 sr for 30 degrees and 0.012 sr for 18 degrees are determined by the monochromator's resolution and the emission angle.

The reason the observed power exceeds predictions based on single particle theory lies in the partial coherence of the emission process. If a Gaussian longitudinal profile is assumed for the beam, the measured power levels are not consistent with the theoretical predictions. Adjusting the pulse length to fit one measurement gives an incorrect prediction for the other measurement. However, if a rectangular longitudinal profile is assumed then not only are the power levels in closer agreement, but the shape of the measurements can also be explained by coherence effects. Rectangular bunch profiles have also recently been suggested to explain the autocorrelation results from coherent transition radiation [16]. Using the method of van den Berg [6] to calculate the values of $|R_{-1}(\theta, 0)|^2$ and assuming a 1% detection efficiency [17], Eq. (2) allows a comparison of the coherent emission to the measured power. The dashed lines in Figs. 4 and 5 indicate the predicted emission from a rectangular microbunch with a length of 19.5 ps and peak current of 1 A. In order to plot the predictions of Eq. (2) in Figs. 4 and 5 a conversion from peak to average power is required. The average power is simply the peak power multiplied by the ratio of the micropulse length to micropulse spacing (19.5/350). Coherence effects are responsible for the major peaks and valleys in the emission while the angular variation of $|R_{-1}(\theta, 0)|^2$ introduces minor variations in the predicted power levels. The location of the peaks are very sensitive to the value of the micropulse length. A 5 percent change in the bunch length results in approximately a 5 percent change in the wavelength which would be easily measureable. As can be seen from Figs. 4 and 5 the levels predicted by assuming a rectangular pulse are approximately 10 times higher than the measured levels for both mirror settings. It is clear however that the peaks and valleys of the predicted and measured power coincide. The premature decline of the signal beyond 1.6 mm is due to a decline in the efficiency of the collection system. The excess in predicted power is most likely due to the fact that the bunch profile lies somewhere between a rectangular and Gaussian distribution, but definitely more rectangular than Gaussian. From Eqs. (2) and (3b) it can be seen that the coherent contribution is larger at 1.32 mm while the incoherent contribution is larger at 0.623 mm. Since the measured power levels are approximately the same for 0.623 mm and 1.32 mm, both the forward enhancement and coherence effects are consistent with the experimental data.

It is interesting to compare the Smith-Purcell emission to a conventional source of far-infrared radiation. A blackbody at a temperature of 5000 K and the same effective area as the grating emits only 0.345 μW in the bandwidth defined in Fig. 5. The Smith-Purcell macropulse signal is more than two orders of magnitude larger than the blackbody. This ratio is similar to that achieved by synchrotron radiation in the far-infrared [18], which in recent years has become a very important tool for Fourier transform spectroscopy research in this spectral regime. Operation of a Smith-Purcell device at shorter wavelengths has also been suggested [19].

The authors would like to thank the staff at the ATF and in particular X. Wang whose efforts made this experiment possible. We also thank M. F. Kimmitt for his assistance in calibration of the detector and for use of his grating monochromator. We gratefully acknowledge support from the U.S. Army Research Office Grant DAAL03-91-G-0189 and the Department of Energy contract DE-AC02-76-CH00016.

[1] S. J. Smith and E. M. Purcell, Phys. Rev. **92**, 1069 (1953).
[2] G. Toraldo di Francia, Nuovo Cimento **16**, 61 (1960).
[3] S. J. Smith, Ph.D. thesis, Harvard University, 1953.
[4] J. Walsh, K. Woods, and S. Yeager, Nucl. Instrum. Methods A **341**, 277 (1994).
[5] J. S. Nodvick and D. S. Saxon, Phys. Rev. **96**, 180 (1954).
[6] P. M. van den Berg, J. Opt. Soc. Am. **63**, 1588 (1973).
[7] O. Haeberlé, P. Rullhusen, J.-M. Salomé, and N. Maene, Phys. Rev. E **49**, 3340 (1994).
[8] G. R. Harrison, J. Opt. Soc. Am. **39**, 522 (1949).
[9] K. Batchelor *et al.*, Nucl. Instrum. Methods A **318**, 372 (1992).

[10] X. J. Wang *et al.*, J. Appl. Phys. **72**, 888 (1992).
[11] G. Doucas, J. H. Mulvey, M. Omori, J.Walsh, and M. F. Kimmitt, Phys. Rev. Lett. **69**, 1761 (1992).
[12] At smaller emission angles a part of the emitted radiation passes below the collection mirror.
[13] G. Doucas, J. H. Mulvey, M. Omori, J.Walsh, and M. F. Kimmitt, Nucl. Instrum. Methods A **331**, 609 (1993).
[14] A. Gover, P. Dvorkis, and U. Elisha, J. Opt. Soc. Am. B **1**, 723 (1984).
[15] M. Goldstein, Ph.D. thesis, Dartmouth College, 1994.
[16] P. Kung, H. Lihn, H. Wiedemann, and D. Bocek, Phys. Rev. Lett. **73**, 967 (1994).
[17] The efficiency of the collection system is based on efficiency measurements made when the collection system was used for the experiments in [11].
[18] G. P. Williams, Rev. Sci. Instrum. **63**, 1535 (1992).
[19] M. J. Moran, Phys. Rev. Lett. **69**, 1761 (1992).

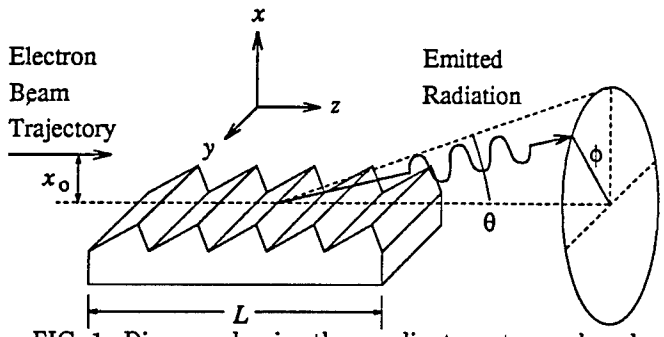

FIG. 1. Diagram showing the coordinate system and angles which define the direction of the emitted radiation. The beam axis is in the z direction, and x is normal to the grating plane. θ is the polar angle, and ϕ is the azimuthal angle.

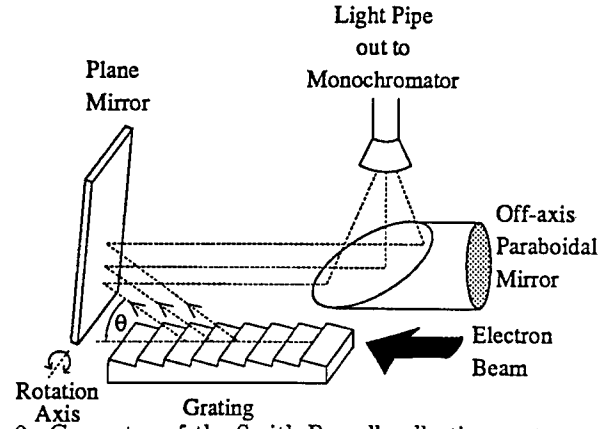

FIG. 2. Geometry of the Smith-Purcell collection system. The dashed lines indicate the path of the emitted radiation and θ defines the emission angle.

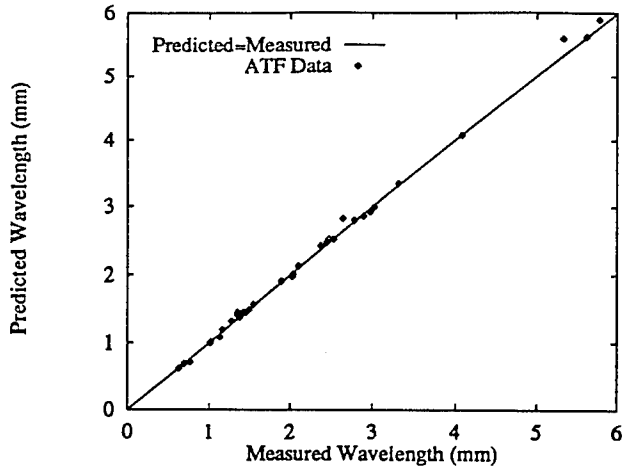

FIG. 3. Plot of predicted vs. experimental wavelengths.

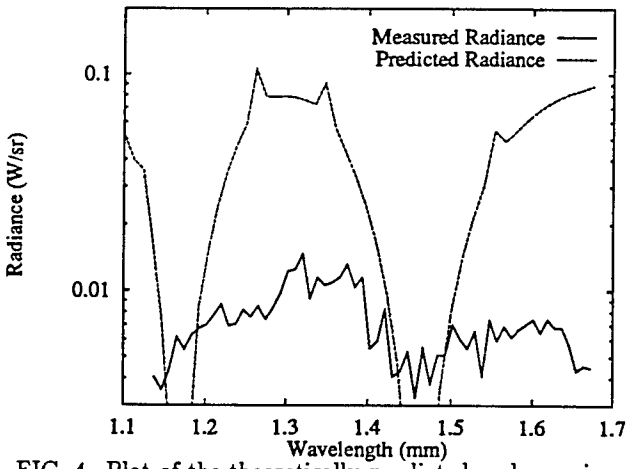

FIG. 4. Plot of the theoretically predicted and experimentally measured radiance at the nominal 30 degree collection angle.

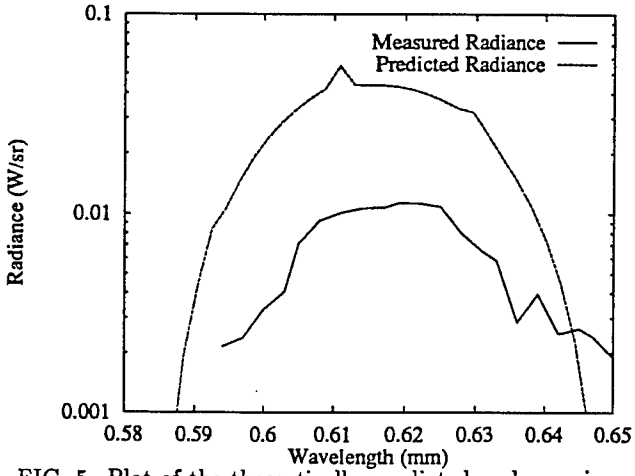

FIG. 5. Plot of the theoretically predicted and experimentally measured radiance at the nominal 18 degree collection angle. The experimental measurements have been scaled by a factor of 2 to account for the radiance from the entire grating.

1994 International Conference on Free-Electron Lasers
Stanford, CA

SMITH-PURCELL RADIATION IN THE RELATIVISTIC LIMIT

Walsh, J.*, Woods, K.*, Stoner, R.**, Fernow, R.†, Kirk, H.†

*Department of Physics and Astronomy, Dartmouth College, Hanover, N.H., **M.I.T., Cambridge, MA, †Brookhaven National Laboratory, Upton, N.Y.

Relativistic peaking of forward-emitted of Smith-Purcell radiation has been observed for the first time. In the original observations of radiation produced by electrons moving at grazing incidence near to the surface of a diffraction grating, Smith and Purcell used a 5 μA, 150 μm diameter, non-relativistic 250-350 kV beam to produce radiation in the visible region of the spectrum. Subsequent work by a number of other researchers used beams to comparable or lower energy. In the non-relativistic limit, short (far-infrared to visible) wavelengths can be achieved with beams of modest energy and gratings with short periods (μm's). The emission is highly dispersed and peaks at angles nearly normal to the grating. Short-wavelength operation can also be obtained by using a relativistic electron beam and a grating with a relatively much longer period. The radiation emitted in this limit is peaked in the forward direction, strongly polarized, and the total spectrum is compressed into a range of angles of the order of the reciprocal of the beam energy. In this limit it is a characteristic double Doppler shift which produces the short-wavelength output.

The experiments which are providing the first evidence of the existence of this operating regime, which is unique to the relativistic limit, are being carried out on the injector section of the ATF accelerator. This is a radio-frequency electron gun equipped with a photo-cathode. It generates a 2.8 MeV beam with a total charge of 1-2 nC spread out over 10-20 micropulses (supercharge mode). To date, the spontaneous component of the emission has been investigated. Like the infrared emission from a synchrotron, which the process resembles, the spontaneous emission is directly useful as a source for Fourier transform spectroscopy. The stimulated component of the emission may also provide the basis of a new type of free-electron laser and optical resonator designs which can exploit the stimulated relativistic Smith-Purcell mechanism are under investigation. Progress on resonator development, results from recent experiments with the ATF injector, and projections for experiments at higher beam energy will be summarized.

Support of U.S. Army Research Office Contract DAAL03-91-K-0189 is gratefully acknowledged.

36th Annual Meeting, APS Division of Plasma Physics
7–11 November 1994—Minneapolis, MN
ABSTRACT SUBMITTAL FORM

Subject Classification Category (refer to DPP Category list) 5.5 ☐ Theory ☒ Experiment

Smith-Purcell Experiments with a Scanning Electron Microscope*, M. GOLDSTEIN and J.E. WALSH Dartmouth College, ---A diffraction grating mounted in the focal region of a scanning electron microscope has been used to produce far-infrared Smith-Purcell radiation. The wavelengths varied between 340 and 730 μm. Beam diameters varied from 10 to a few 10's of μm and the voltage and current ranges were 30-40 kV and 10-60 μA. The power levels of the radiation at the detector were 10's of pW. Collection efficiency of the present optical system is of the order of 1% and thus the generated power is some 10's of nW. These levels are modest but comparable to, or in excess of, the intensity levels available from a blackbody source in the same spectral range. Both the wavelengths and the intensity observed are in accord with expectations based on theory. The details of the experiment and the implications the results have on the challenge of developing a new class of vacuum microelectronics coherent, far-infrared radiation sources will be discussed.

*Support of ARO Contract # DAAL03-91-G-0189 and Vermont Photonics, Inc. is gratefully acknowledged.

☒ Prefer Poster Session
☐ Prefer Oral Session
☐ This poster/oral should be placed in the following grouping: (specify order)

☐ Special Audiovisual Requests (e.g., movie projector)

☐ Other Special Requests

Submitted by:

John E. Walsh
(Signature of APS Member)

John E. Walsh
(Same Name Typewritten)

Dartmouth College
Department of Physics & Astronomy
6127 Wilder Laboratory
Hanover, N.H. 03755-3528
(Address)

A faxed copy is NOT acceptable. This form, or a computer-generated form, plus TWO COPIES, must be received by **Friday, 8 July 1994** at the following address:

Saralyn Stewart
The University of Texas at Austin/Institute for Fusion Studies
26th and Speedway–RLM 11.234
Austin, TX 78712
Phone (512) 471-4378

36th Annual Meeting, APS Division of Plasma Physics
7–11 November 1994—Minneapolis, MN
ABSTRACT SUBMITTAL FORM

Subject Classification Category (refer to DPP Category list) 5.5 ☐ Theory ☒ Experiment

Forward Peaking of Relativistic Electron-Beam-Generated Smith-Purcell Radiation*, K.J. WOODS , Dartmouth College, R.E. Stoner, M.I.T., R. Fernow, H. Kirk and J.E. WALSH, Brookhaven National Laboratory----Recent experiments carried out with a 2.8 MeV electron beam have provided the first experimental evidence of forward peaking of Smith-Purcell radiation in the relativistic limit. The beam was produced with the injector section of the 50 MeV ATF linac at Brookhaven National Laboratory. Radiation in a wavelength band extending from 1.1 - 1.65 mm and in a region around 623 μm has been generated with the 750 μm x 2.5 cm cross-section beam moved over a 1 cm period grating. The grating had a 5° blaze and an échelle profile. It was 17 periods long. The emission angles were 30° and 18° respectively and these observations are consistent with expectations based on the Smith-Purcell wavelength formula. The 623 μm signal was somewhat more intense than 1. - 1.6 mm radiation and this, too, is consistent with theoretical expectations. The details of the experiment will be presented and the implications for developing polarized sources with strong forward peaking will be reviewed.

*Support of ARO Contract # DAAL03-91-G-0189 and the Brookhaven National Laboratory ATF project are gratefully acknowledged.

☒ Prefer Poster Session
☐ Prefer Oral Session
☐ This poster/oral should be placed in the following grouping: (specify order)

_____
_____

☐ Special Audiovisual Requests (e.g., movie projector)

_____
_____

☐ Other Special Requests

_____
_____

Submitted by:

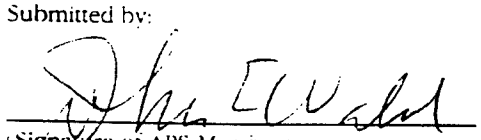

(Signature of APS Member)

John E. Walsh

(Same Name Typewritten)

Dartmouth College
Department of Physics & Astronomy
6127 Wilder Laboratory
Hanover, N.H. 03755-3528

(Address)

A faxed copy is NOT acceptable. This form, or a computer-generated form, plus TWO COPIES, must be received by **Friday, 8 July 1994** at the following address:

Saralyn Stewart
The University of Texas at Austin/Institute for Fusion Studies
26th and Speedway–RLM 11.234
Austin, TX 78712
Phone (512) 471-4378

36th Annual Meeting, APS Division of Plasma Physics

7–11 November 1994—Minneapolis, MN

ABSTRACT SUBMITTAL FORM

Subject Classification Category 5.5 (refer to DPP Category list) ☐ Theory ☒ Experiment

Smith-Purcell Radiation in the Relativistic Limit*, J.E. WALSH, S.G. YEAGER and K.J. WOODS, Dartmouth College,----A "strip"-grating-based theoretical model has been developed for the purpose of investigating the general features of Smith-Purcell radiation in the relativistic limit. Although idealized, the model has the advantage of yielding analytic expressions for the intensity and angular distribution of the radiation. The conditions under which a characteristic high-energy forward peaking of the emitted radiation have been identified explicitly, and comparison with other highly-collimated, polarized *continuum* sources (such as undulator and synchrotron radiation) is under way. When beam energy, current and emittance values typical of free-electron laser linacs are used as a starting basis for comparison, the intensity of the *continuum* emission from a grating at infrared and far-infrared wavelengths is expected to exceed that available on an infrared beamline on a synchrotron. The model is also being used to explore the gain parameter space available to linac-driven Smith-Purcell free-electron lasers. A discussion of a planned series of experiments to be carried out with 40-50 MeV linacs will be presented.

*Support of ARO Contract # DAAL03-91-G-0189 and Vermont Photonics, Inc. is gratefully acknowledged.

☒ Prefer Poster Session
☐ Prefer Oral Session
☐ This poster/oral should be placed in the following grouping: (specify order)

_____

_____

☐ Special Audiovisual Requests (e.g., movie projector)

_____

_____

☐ Other Special Requests

_____

_____

Submitted by:

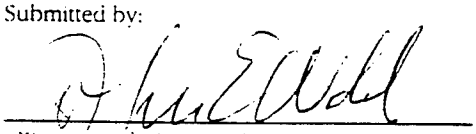

(Signature of APS Member)

John E. Walsh

(Same Name Typewritten)

Dartmouth College
Department of Physics & Astronomy
6127 Wilder Laboratory
Hanover, N.H. 03755-3528

(Address)

A faxed copy is NOT acceptable. This form, or a computer-generated form, plus TWO COPIES, must be received by **Friday, 8 July 1994** at the following address:

Saralyn Stewart
The University of Texas at Austin/Institute for Fusion Studies
26th and Speedway–RLM 11.234
Austin, TX 78712
Phone (512) 471-4378

Abstract Submitted
for the Spring Meeting
of the American Physical Society
April 18-22, 1994

Smith-Purcell Radiation in the Relativistic Electron Beam Limit*, J. WALSH and K. WOODS, Dartmouth College, R. STONER, MIT, R. FERNOW, H. KIRK and X. WANG, Brookhaven National Laboratory,--- Observations of radiation produced by electrons skimming over a grating were first reported by Smith and Purcell [1]. The equation

$$\lambda = \ell \left(\frac{1}{\beta} - \cos\theta\right) \qquad (1)$$

relating wavelength λ, grating period ℓ, relative velocity of the electrons β, and the angle of emission, was also discussed in [1]. In [1] and most, but not all [2], subsequent experiments, beams of moderate energy were employed. Equation (1) of course remains valid as $\beta \rightarrow 1$. As $\theta \rightarrow 1/\gamma$ ($(\gamma - 1 = eV_b/mc^2)$, large "upshifts" ($\ell/\lambda >> 1$c peaking of the radiation are to be expected. It can be shown that when terms which depend explicitly on the grating profile are grouped separately, the remaining factors which control the coupling are summarized by the expression:

$$F_c \equiv \left(\ell^3/\lambda^3\right) \sin^2\theta(\lambda)\ e^{-2\pi b/\lambda\beta\gamma} \qquad (2)$$

and it follows that the ratio of the relative impact parameter (b) and the grating period be comparable or smaller than γ^{-1}. The theoretical basis of Eq. (2) will be discussed and results from recent experiments in which operation at $\ell/\lambda >> 1$ has been demonstrated will be presented.

*Support of ARO Contract # DAAL03-91-G-0189 and ATF staff are gratefully acknowledged.

[1]. Phys.Rev. **92**, 1069 (1953).
[2]. Phys.Rev.Lett. **69**(12), 1761 (1992).

Signature of APS Member

John E. Walsh
Dartmouth College
Department of Physics and Astronomy
6127 Wilder Laboratory
Hanover, N.H. 03755-3528

( ) Prefer Oral Session

Abstract Submitted

A Millimeter Wavelength Radiation Source Using a DualGrating Resonator

J. H. Killoran, F. L. Hacker, and J. E. Walsh

Abstract—A novel means of producing coherent radiation by passing an electron through a dual-grating resonator is presented. The observed radiation is in accordance with the Smith-Purcell dispersion relation for a single grating. Feedback is provided by a second grating. Experiments carried out at beam energies from 30-55 KeV produced radiation at wavelengths from 6 to 0.75 mm. Power measurement were used to clarify the grating-beam interaction. Indications are that operation could be easily extended to shorter wavelengths to provide an inexpensive and compact radiation source in the far-infrared.

I. Introduction

THE term Orotron [1] is used generally to describe a coherent radiation source which employs an open quasi-optical resonator to store energy generated by an electron beam as it moves over a diffraction grating. In its original form the resonator was completed by a spheroidal mirror placed on an axis normal to the grating. Radiation was extracted through an aperture in the mirror. Typical operating wavelengths of these devices fall in the mm to upper sub-mm region of the spectrum.

The electron beam as it traverses the grating actually emits over a range of angles and wavelengths related to beam and grating parameters by the well known Smith-Purcell formula [2]. Mizuno [3] in a device he termed the Ledatron reported on observations of a surface mode which produced radiation along the direction of beam propagation.

A variation of the device termed a planar Orotron [4]-[6] has also been investigated. In this version of the Orotron a planar strip grating is embedded in an open sided parallel plate wave guide. The resonator is completed with cylindrical section mirrors (Fig. 1). Radiation is extracted along the beam axis through an aperture in the mirror. Operation of the planar Orotron has been extended [5] to 750 GHz (400 μm). Ultimately cavity Q is limited by the apertures and a portion of the power produced is emitted counter to the beam through the beam entrance aperture. The resonator introduced in this work employs a second grating as a feedback element which circumvents these constraints by shifting the optical axis away from the axis of the electron beam. It is similar in this respect to the original version of the Orotron but unlike those structures the choice of emission angle, and thus wavelength, is not restricted.

Manuscript received September 13, 1993; revised February 16, 1994. The support of the US Army Research Office DAAL03-91-G-0189 is gratefully acknowledged.

The authors are with the Department of Physics, Dartmouth College, Hanover, NH 03755 USA.

IEEE Log Number 9404575D.

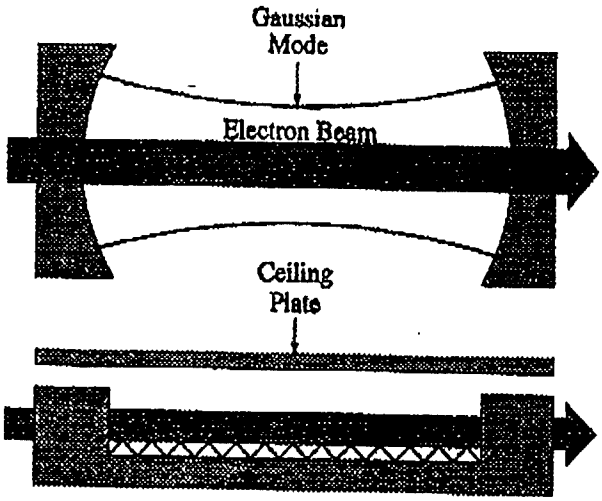

Fig. 1. Confocal Resonator Configuration.

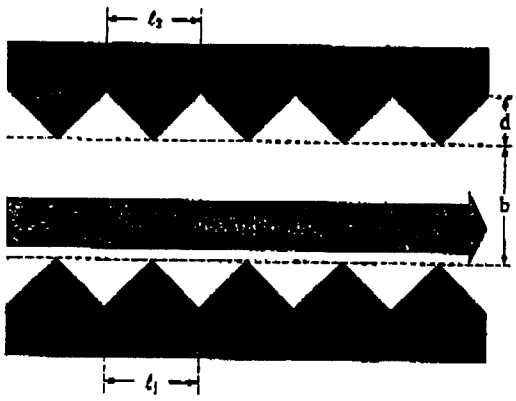

Fig. 2. Dual Grating Resonator.

II. The New Resonator: Background

The geometry of our new resonator is shown in Fig. 2. Of the two gratings employed, only one interacts with the beam so that radiation is emitted at an angle to the grating surface. It will be shown that the emitted wavelength is described by, [2]

$$\lambda_{sp} = \frac{\ell}{n}(1/\beta - \sin\theta), \tag{1}$$

where λ_{sp} is the wavelength of the spontaneous radiation emitted at an angle θ with respect to the grating normal, and β is the relative velocity of the electron beam which passes over a grating of period ℓ. The integer n is the relative order of the emitted radiation.

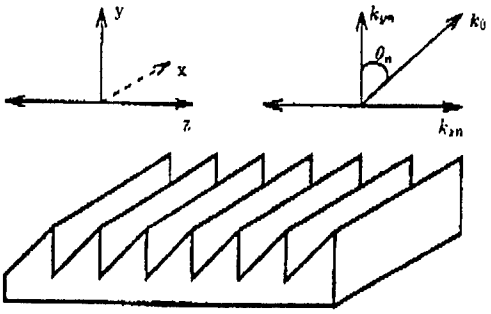

Fig. 3. The Coordinate System Used for Mathematical Treatment of Gratings.

While (1) describes radiation emitted spontaneously, another model is needed to describe the coupling between the electron beam and the fields above the grating surface. We consider a TM electromagnetic wave, with time dependence $e^{i\omega t}$, which propagates along the grating surface with a propagation constant k_{z0}. Fig. 3 shows the coordinate system used in relation to the grating which is considered to be infinite in the x direction. The magnetic field can be expressed as a sum of *spatial harmonics:*

$$\mathbf{H}(y,z) = \sum_{n=-\infty}^{n=\infty} H_n(y) e^{i(k_{z0}+\frac{2\pi n}{\ell})z}\hat{x}. \tag{2}$$

Each term of this expansion must also be a solution to the Helmholtz wave equation. Dropping the vector notation for convenience, we arrive at the expression,

$$H(y,z) = \sum_{n=-\infty}^{n=\infty} H_n e^{ik_{yn}y} e^{ik_{zn}z} \tag{3}$$

where

$$k_{zn} = k_{z0} + \frac{2\pi n}{\ell} \tag{4}$$

$$k_{yn} = (k_0^2 - k_{zn}^2)^{\frac{1}{2}} \tag{5}$$

and $k_0 = \omega/c$. Terms of (3) for which k_{yn} is real propagate away from the grating surface at an angle $\theta_n = \tan^{-1}(k_{zn}/k_{yn})$ measured with respect to the grating normal. Harmonics for which k_{yn} is complex are evanescent, meaning they decay away exponentially from the grating surface. The relative magnitude of the spatial harmonics H_n depends on the the boundary conditions of the specific grating profile used. Solving for these coefficients is a difficult problem which must, in general, be done numerically. Once $\mathbf{H}(y,z)$ is known, the electric field components follow trivially.

Once an expression for the fields is known, coupling between fields and the electron beam can be calculated according to:

$$\frac{d\mathcal{E}_{\text{mech}}}{dt} = \frac{1}{2}\int_V \mathbf{J}^* \cdot \mathbf{E}\, d^3x. \tag{6}$$

Energy transfer from the beam to the radiation field is most efficient when the velocity of the electron beam is slightly greater than the phase velocity of the wave, so that

$$v_{\text{beam}} \simeq \omega/k_{zn}. \tag{7}$$

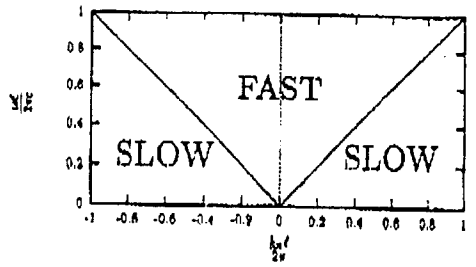

Fig. 4. The Dispersion Plane.

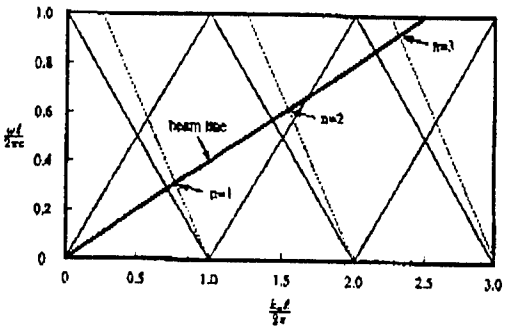

Fig. 5. Dispersion Plane Representation of Smith Purcell Emission.

Clearly, this can only be satisfied for spatial harmonics with phase velocities such that $\omega/k_{zn} = v_{ph} < c$ and k_{yn} is complex. This condition is graphically represented by the *slow* region of the dispersion plane shown in Fig. 4. The units used in this graph are scaled with the grating period ℓ such that a wave propagating with phase velocity c is denoted by a line of slope 1. Similarly, an electron beam with velocity v can be denoted by a line of slope $\beta = v/c$. Using (7), the Smith-Purcell relation (1) can be rewritten as

$$\frac{k_{zn}\ell}{2\pi} = \frac{\omega\ell}{2\pi c}\sin\theta + n. \tag{8}$$

Output of the n^{th} order at a given angle θ can be graphically represented by the intersection of (8) and the 'beam line' as shown in Fig. 5 for $\theta = -45$ degrees.

Of the two gratings used, only one serves to provide the stimulus for radiation emission. The function of the second grating is to return this radiation to the surface of the first grating such that two gratings together form a resonant cavity. How this can be achieved is best illustrated using the diffraction grating formula,

$$m\frac{\lambda}{\ell} = \sin\theta_i + \sin\theta_m. \tag{9}$$

This equation describes the diffraction of a plane wave of wavelength λ incident on a grating of period ℓ at an angle to the grating normal given by θ_i. The wave will then be diffracted into various orders given by the integer m at angle θ_m. The number of diffracted orders is determined by the value of λ/ℓ. For $\lambda/\ell > 2$ only the $m = 0$ order exists and all incident radiation is specularly reflected ($\theta_i = -\theta_m$). The specific grating profile determines the distribution of the incident radiation into multiple diffracted orders [7].

For a Littrow configuration, the incident wave diffracted into the m^{th} order is always returned at the incident angle,

and the grating behaves like a mirror. The Littrow angles are specified by $\theta_i = \theta_m$, so equation 9 becomes

$$m\frac{\lambda}{\ell} = 2\sin\theta_i. \tag{10}$$

While some radiation is inevitably diffracted into the $m = 0$ order, it has been shown that for the echelette profile the efficiencies for Littrow configured gratings can approach unity when the radiation is incident at an angle normal to the grating tooth [8].

It should be noted, that the diffraction theory presented here is not a complete description of the present device. The dual grating resonator has only been shown to operate when the distance separating the gratings is comparable to the evanescent length of the slow spatial harmonics defined in (3) ($\ell/b \sim k_{yn}\ell/2\pi$). Therefore, the gratings are not independent and (3) is a simplification. In particular, output radiation has been observed for which $\lambda/\ell > 2$, a wavelength at which Littrow reflection is not possible. Operation does follow a simple and predictable pattern, as shall be shown.

III. Apparatus

The Dartmouth College Plasma Lab *Planar Orotron* utilizes a Pierce type electron gun to generate an electron beam. A 30 KV power supply is used to charge 1000 feet of RG-8U coaxial cable which serves as a large capacitor with an approximately 1.5 μs discharge time. The capacitor is rapidly discharged to form a high voltage pulse which is stepped up by a 12:1 ratio. Electrons are emitted across an A–K gap formed by a Barium Oxide impregnated Tungsten matrix cathode and a carbon graphite anode held at ground potential. The repeat rate is adjustable but is generally set at around 1 Hz. Beam energies over 200 keV can be attained.

Fig. 6(a) and 6(b) show the dimensions of the resonator used for our experiments. Essentially, the resonator is formed by two gratings held together in a two part mount with fixes them in position. Both the mount and gratings are made of aluminum. Two carbon blocks, mounted at the entrance to the resonator, serve to 'trim' the beam to a roughly rectangular profile 0.150 in. thick. At the opposite end, the electron beam and output radiation exit the resonator and pass into a section of WR-28 waveguide where the electron beam is diverted by a small fixed magnet and 'dumped' onto the walls of the guide. Output radiation continues on and leaves the vacuum chamber through a teflon window and can then be detected and characterized.

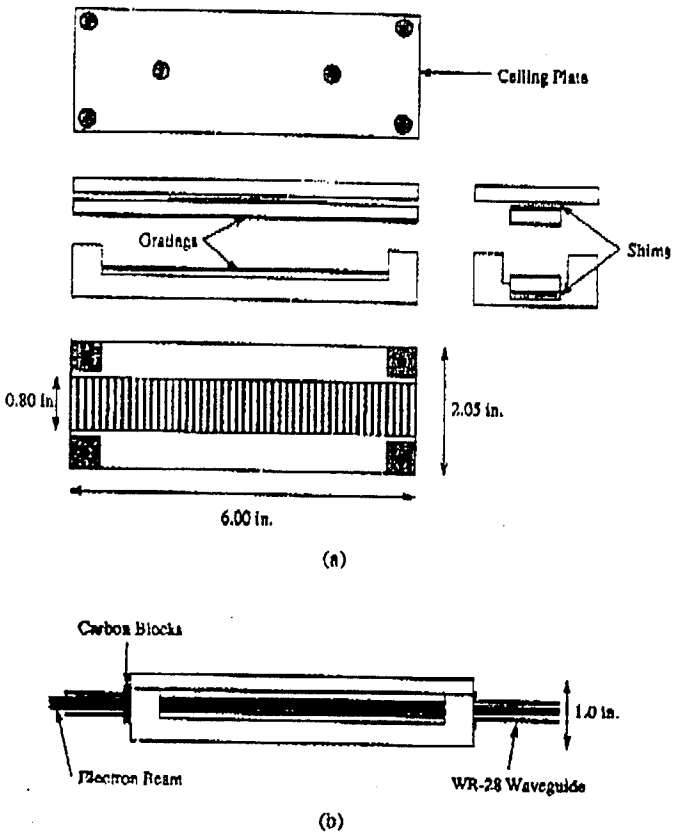

Fig. 6. (a) The double grating resonator (scale drawing) (b) The double grating resonator in operation (scale drawing).

Table I. Double Grating Resonator Configurations Used

Configuration	Grating 1	ℓ_1 (mm)	Grating 2	ℓ_2 (mm)
A	Sawtooth	1.524	Echelette	1.524
B	Sawtooth	3.048	Echelette	1.524
C	Sawtooth	1.524	Echelette	0.762
D	Sawtooth	0.762	Echelette	0.762

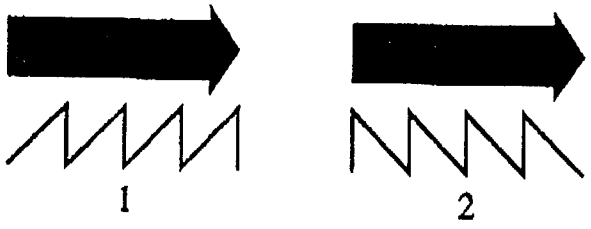

Fig. 7. Sawtooth Grating Orientations Used.

IV. The New Resonator: Operation

Table I lists the four different grating combinations used in our experiments. The profiles of both gratings were chosen to maximize the efficiency of radiation incident at 45 degrees to the normal. The echelette profile, blazed at 45°, was always used as grating #2 because it has been shown theoretically and experimentally to be highly efficient, particularly when used as a Littrow mount [8]. The 'sawtooth' profile was also chosen because it had been used in previous research [5] and had been shown to have desirable gain characteristics. For this work, the sawtooth profile is defined as any triangular profile which has a non-apex angle of 90°. Unlike echelette gratings, the sawtooth profile is always antisymmetric. Experiments were run with both orientations of the sawtooth profile with respect to the electron beam as shown in Fig. 7.

Output radiation was measured using two different detectors, a diode and a Liquid Helium cooled InSb electron bolometer. Both detectors provide an output signal roughly proportional to the output power. While the diode detector needs no cooling, it rapidly looses sensitivity at frequencies over 100 GHz. The bolometer provides fairly uniform sensitivity from 30-1200 GHz [9].

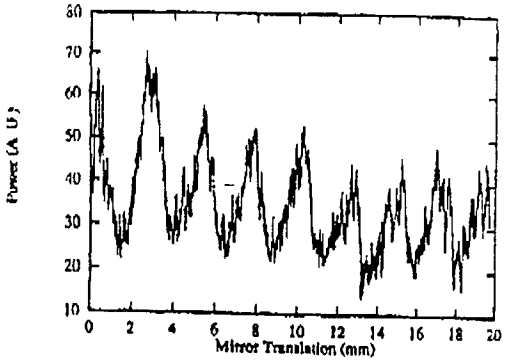

Fig. 8. An interferogram of unfiltered data.

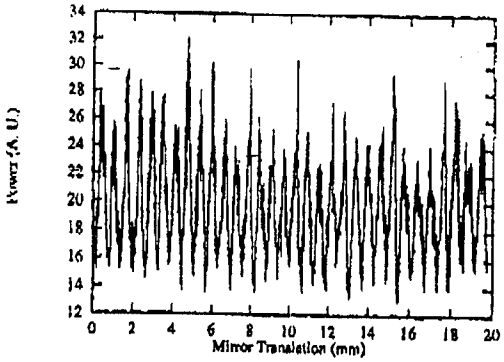

Fig. 10. Interferogram made with high pass filter in place.

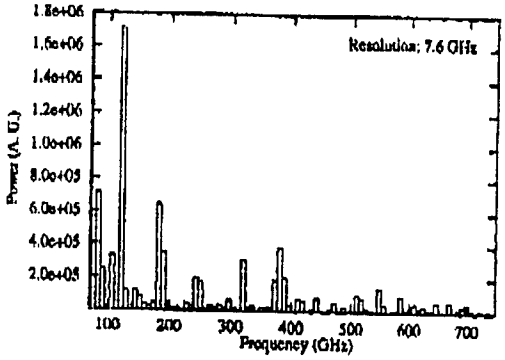

Fig. 9. Fourier transform of unfiltered data.

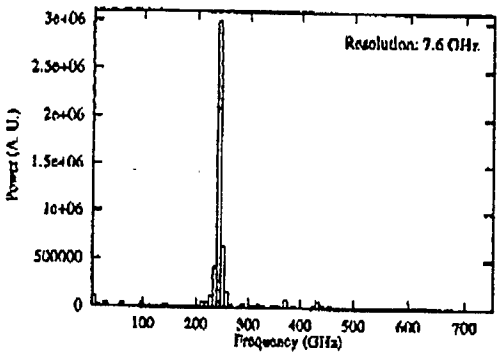

Fig. 11. Fourier transform of filtered output.

Frequency measurements were made with a Michelson interferometer, and the spectral content analyzed using a discrete Fourier transform. In virtually all cases, multi-mode operation was observed, with power levels sharply decreasing for the higher frequency modes. Fig. 8 shows an interferogram taken using resonator configuration A. The lowest order frequency component is highly dominant and higher frequency components are not apparent by inspection, but are revealed using a Fourier transform in Fig. 9. The dominant $n = 1$ component not shown in the figure is at 61 GHz and has a magnitude of $2.4 \times 10^{+7}$. A second interferogram, made using a 250 GHz high pass filter is shown in Fig. 10 and it's corresponding Fourier transform in Fig. 11. While in principal the filter removes only the frequency components below 250 GHz, it does appear that the modes about 300 GHz have been sharply attenuated as well. This is most likely due to small shifts in the beam velocity between measurements, since individual modes tend to strongly prefer highly specific beam energies.

By assuming synchronous coupling with the electron beam, the data can be reduced and plotted on the dispersion plane as shown in Fig. 12. The diagonal line through each data point represents the uncertainty due to the resolution of the interferometer. This exceptional data recorded seven simultaneous modes of operation, about twice the number typically observed. On the basis of the measured frequency, the beam velocity, and (7), an effective 'emission' angle can be calculated. The data shown is typical because each mode falls near one of the lines corresponding to Smith-Purcell 'emission,' at a particular angle θ, in this case either -45 or $+45$ degrees.

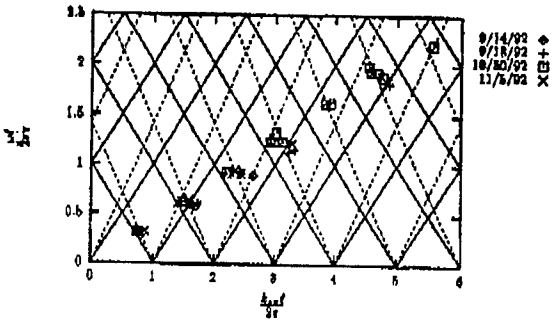

Fig. 12. An example of reduced data: Resonator configuration A.

Table II summarizes the frequency data for the various resonator configurations. Resonator configuration A was used for the majority of the data collected, and perhaps this is why more modes have been observed with it. The starred entries under Configuration C indicate a possible ambiguity in the scaling of frequencies with grating period introduced by the two different grating periods used. Close examination of the data indicates that a high frequency mode observed using this configuration may have been due to a lower order mode excited by the shorter period grating. Infrequently, a mode of operation below the $n = 1$ mode, denoted by $n = 0$ in Table II, was observed. All spatial harmonics of this mode are evanescent, therefore the second grating does not provide any feedback. This mode probably operates because the end of the grating is seen by the wave as a discontinuity and causes substantial reflection, enough to form a resonant cavity.

Another measurement of interest the *Start Oscillation Current* (I_{start}) which is the minimum current necessary to gener-

TABLE II
SUMMARY OF FREQUENCY MEASUREMENTS

Configuration	Modes Observed	Output Frequencies,(GHz)
A	(1) - (7)	62,122,182,243,319,380,432
B	(0),(2),(3),(4)	32,80,120,160
C	(0),(1),(2),(2*)	51,60,118,240*
D	(1),(2),(3)	125,249,374

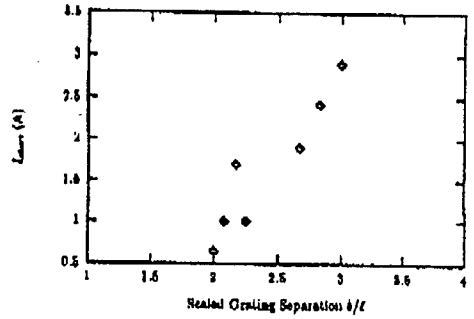

Fig. 13. Start oscillation current versus grating spacing: Configuration A.

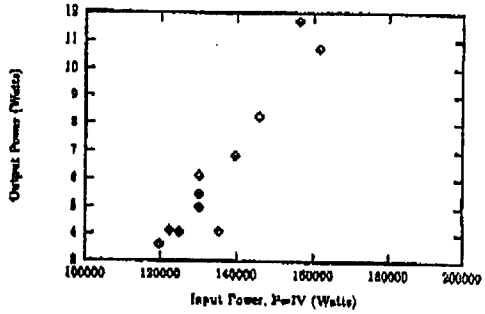

Fig. 14. Output power versus input power: Configuration A.

ate sufficient radiation to overcome the inherent cavity losses. The value of I_{start} should be inversely proportional to the resonator quality factor Q Previous research at Dartmouth [10], using a confocal resonator, demonstrated the dependence of I_{start} on cavity Q. Metal meshes were used to cover the output apertures, and increase cavity Q, resulting in reduced start currents. For the dual grating resonator, the measured start currents were sensitive to small adjustments of the gratings. The dominant trend was that I_{start} increased with grating separation b, —spaceas shown in Fig. 13 for resonator configuration A. Precise comparison with specific Q values is extremely difficult using the present beam generator.

Fig. 14 shows output radiation power as a function of input electron beam power measured by varying the current for a fixed electron beam energy. These power measurements were made using the $n = 1$ mode of resonator configuration A tuned to approximately 65 GHz. A convenient, calibrated source was available at that frequency. The rate of increase of power with current clearly indicates that the device is not operating at saturation. While these power levels are respectable for sources of this type, the efficiencies are very low ($\sim 3 \times 10^{-5}$). However, operating efficiencies could be dramatically improved if a recapture scheme were in place to utilize the considerable amount of energy left in the electron beam once it leaves the resonator.

V. SUMMARY

Experimental results from a new type of resonator for use as an electron beam driven radiation source are presented. The device operates in multiple modes, each at a discrete frequency. A simple model assuming synchronous coupling of a TM wave to the electron beam shows a distinct correlation between each mode of operation and harmonics emitted according to the Smith-Purcell equation. The radiation ranged in output frequency from 50–400 GHz. Power levels decreased sharply with increasing frequency. For the lowest order modes, power levels were observed in the range of 10 W. The rate of increase of output power with current indicates that the device is not operating at saturation. The decrease in power at shorter wavelengths is mainly the result of the decreasing fraction of the beam being used to drive the cavity. As λ decreases, the coupling terms of the electromagnetic field decay away more rapidly with increased distance from the grating surface. The result is that an ever greater portion of the beam passes 'too high' above the grating surface to be effectively utilized. This trend can be compensated for by using higher charge density electron beams.

These proof-of-principal resonators set the foundation for future work using higher Q cavities to reduce the start oscillation current and improve mode selectivity. It is expected that improved resonator designs, and better electron beam generation, will result in higher attainable output frequencies.

ACKNOWLEDGMENT

Thanks are due to Dr. Emily Fisch for her assistance in preparing this document.

REFERENCES

[1] F. S. Rusin and G. D. Bogomolov, "Orotron—an electronic oscillator with an open resonator and reflecting grating," in *Proc. of the IEEE*, vol. 57, pp. 720–722, 1969.
[2] S. J. Smith and E. M. Purcell, "Visible light from localized surface charges moving across a grating," *Physical Rev.*, vol. 92, p. 1069, 1953.
[3] K. Mizuno and S. Ono, "The ledatron," in K. Button, Ed., *Infrared and Millimeter Waves 1: Sources of Radiation*, New York: Academic Press, Inc., 1979, ch. 5, pp. 213–233.
[4] E. E. Fisch, "The sapphire Cerenkov laser," *Ph.D. Thesis*, Dartmouth College, 1991.
[5] F. J. Price, "Operation of a Smith-Purcell free-electron laser at submillimeter wavelengths," *Ph.D. Thesis*, Dartmouth College, 1991.
[6] P. M. Phillips, "Planar orotron: a tunable grating-based free-electron laser," *Ph.D. Thesis*, Dartmouth College, 1987.
[7] T. M. Hard, "Laser wavelength selection and output coupling by a grating," *Applied Optics*, vol. 9, pp. 1825–1830, 1970.
[8] D. Maystre, M. Neviere, and R. Petit, "Experimental verifications and applications of the theory," Ed., R. Petit, *Electromagnetic Theory of Gratings*, New York: Springer-Verlag, 1980, ch. 6. .
[9] M. F. Kimmitt, *Far-Infrared Techniques*, Pion Limited, 1970, ch. 4, p. 79.
[10] J. A. Jackson, "The Planar orotron: a metal grating coupled, millimeter wavelength radiation Source," *Ph.D. Thesis*, Dartmouth College, 1990.

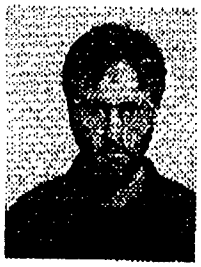

Joseph H. Killoran was born in New York City on August 22, 1966. He received an A.B. in physics from Bowdoin College, Brunswick, ME, in 1988 and recently completed a Ph.D. in Experimental Physics at Dartmouth College. His research has centered around experimental and theoretical aspects of the planar Orotron, a grating coupled free electron laser. He is a member of the American Physical Society.

Fred L. Hacker was born in Wolfeboro, NH on August 18, 1966. He received the B.S. degree in physics from Bates College, Lewiston, ME, in 1988. He is currently working towards the Ph.D. degree in physics at Dartmouth College, Hanover, NH. His present research is on mode locking in a grating coupled free-electron laser.

John E. Walsh was born in New York, NY, on August 20, 1939. He received undergraduate training in electrical engineering at St. Mary's University, Halifax, Nova Scotia, and Nova Scotia Technical College, Halifax, and the graduate degrees in electrical engineering and plasma physics from Columbia University, New York, NY.

From 1962 to 1965 he was a member of the Technical Staff in the Army Signal Corps Laboratory, Ft. Monmouth, NJ. Since 1968 he has been a member of the faculty in the Department of Physics and Astronomy, Dartmouth College, Hanover, NH. His present research interests are the free-electron laser, millimeter-wave sources, and electromagnetic scattering at millimeter wavelengths.

Reprinted from

NUCLEAR INSTRUMENTS & METHODS IN PHYSICS RESEARCH
Section A

Nuclear Instruments and Methods in Physics Research A 341 (1994) 277–279
North-Holland

Intensity of Smith–Purcell radiation in the relativistic regime

J. Walsh *, K. Woods, S. Yeager
Department of Physics and Astronomy, Dartmouth College, Hanover, NH 03755, USA

N·H
ELSEVIER

is determined by the usual boundary conditions. In Eq. (4), y is the dimension along the grating slot and b, the "impact parameter", lies along the x-axis. The spatial extent of the footprint of the electron along the direction of propagation scales in proportion to the reciprocal of the relative energy (γ^{-1}). On a smooth surface, no radiation is produced by current

$$j = v\sigma. \tag{5}$$

When the surface is broken up into strips, however, the situation is modified. The strip grating acts as a spatial switch which produces an on–off modulation which "slides through the charge" at velocity $c\beta$. A modulated current results and a radiative boundary condition (Eq. (2a)) is now satisfied.

The standard expression [10] relating current and radiation can then be used to estimate the power radiated. The integrations required are straightforward. The contribution from the y-dependence yields a modified Bessel function which is sharply peaked in the x–z plane. The region of interest is thus near to the plane defined by the emission angle and the beam axis. Carrying out the remaining integrations then yields:

$$\frac{\mathrm{d}^3 I}{\mathrm{d}\phi\ \mathrm{d}z\ \mathrm{d}\omega} = \frac{2e^2\omega}{\pi^2 c^2}\sin^2\theta\ \exp\left[\frac{-2\omega b}{c\beta\gamma}\right] \tag{6a}$$

or

$$\frac{\mathrm{d}^2 I}{\mathrm{d}z\ \mathrm{d}\Omega} = \frac{4e^2}{\pi l^2}\frac{\sin^2\theta}{(1-\beta\cos\theta)^3} \times \exp\left[-\frac{4\pi b/l}{\gamma(1-\beta\cos\theta)}\right]. \tag{6b}$$

Eq. (4a) is the energy per unit azimuthal angle per unit length of a path per unit angular frequency (b is the impact parameter of the electron). The structure of the formula emphasizes the similarity of the Smith–Purcell radiation and Cherenkov radiation in a dielectric half-space. The second of Eqs. (4) follows when Eq. (3) is used to relate $\mathrm{d}\omega$ with the differential solid angle. When the condition

$$\left.\frac{4\pi b/l}{1-\beta\cos\theta}\right) \lesssim 4 \tag{7}$$

is met, Eq. (4) will display strong peaking in the forward ($\theta \sim 1/\gamma$) region. Representative examples are shown in Fig. 2.

The power scaling of the radiation produced by a beam follow from Eqs. (4) if e^2 is replaced by eI_b, where I_b is the beam current. The coefficient of Eq. (4b) is then

$$\frac{4eI_b}{\pi l^2} = \frac{183 I_b(A)}{l^2(\mathrm{cm})}\ \mathrm{nW/cm\text{-}sr}. \tag{8}$$

The power level of the spontaneous emission is modest, but it exceeds by a large margin the black-body

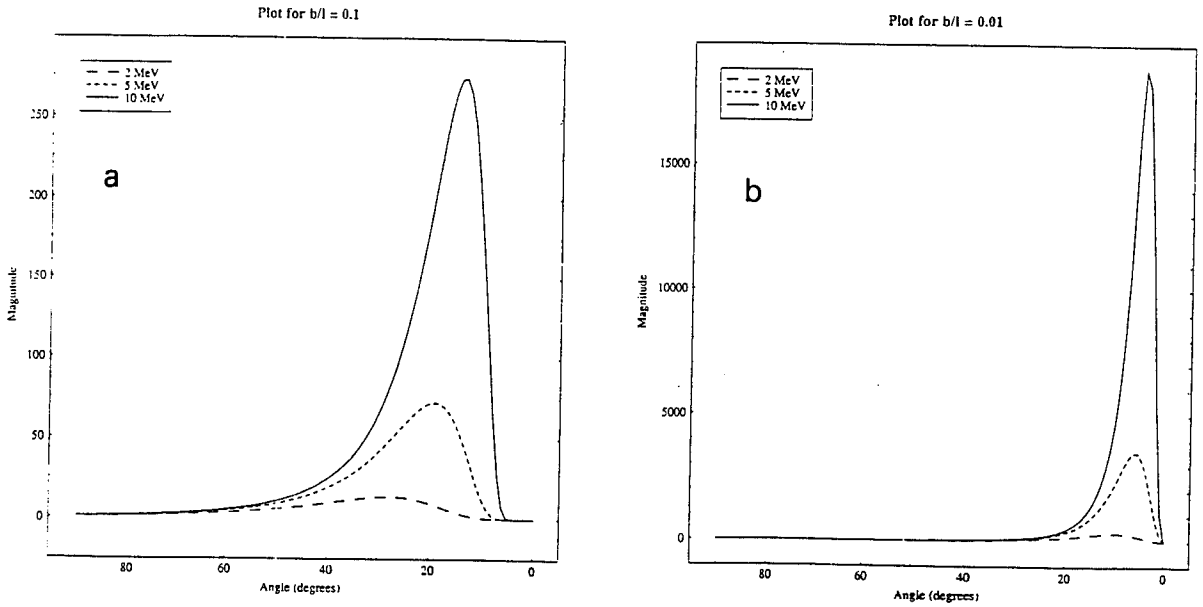

Fig. 2. Typical angular distributions for two values of b/l, 0.1 (a) and 0.01 (b).

emission in the longer wavelength part of the far-infrared. In addition, like the far-infrared beam line on a synchrotron, in the relativistic limit, the Smith–Purcell radiation is strongly polarized and highly peaked. The spontaneous emission is in itself a potentially useful source for Fourier transform spectroscopy. The process may also be the basis of a free-electron laser.

3. Recent experiments

The experiments summarized in ref. [2] yielded (spontaneous) Smith–Purcell radiation which was tunable over a range from a few mm down to approximately 300 μm. The lower-wavelength limit was not a fundamental constraint, but a result of the detectors used and the geometry of the system used to collect the radiation emitted from the grating.

The interaction chamber used for the work described in ref. [2] has now been installed on a beam line at the ATF facility in Brookhaven National Laboratory (ATF-BNL). The ATF-BNL is a photocathode injector-driven linac, and the beam brightness is substantially greater than the Van de Graaff accelerator used in the experiments conducted at Oxford. The principal goals are now to verify the existence of forward peaking and examine options for Smith–Purcell free-electron lasers.

4. Conclusions

The theory introduced above is based on very simple assumptions and in this sense, it is complementary to calculations which begin from a detailed [11–16] consideration of scattering from a grating. It has the virtue of clearly displaying its dependence on the parameters of the experiment. It also points up a result which is at first surprising: In order to maintain good coupling of a beam with a grating at short wavelengths, it is necessary to minimize the impact parameter (b, the mean distance to beam in a typical experiment), and increase the period along with the beam energy. The first of these conditions is obvious but the second is, at first, surprising. The relationship implied by Eqs. (4) yields for a final scaling $\lambda \sim l/\gamma^2 \sim \pi b/\gamma$. Since $0.1 \leq b < 1$ mm fall within the achievable focussing tolerance of moderate-energy, high-quality linacs, operation in the infrared–far-infrared regions of the spectrum are a realistic possibility.

Acknowledgement

Support of the U.S. Army Research Office Grant DAAL03-91-G-0189 is gratefully acknowledged.

References

[1] S.J. Smith and E.M. Purcell, Phys. Rev. 92 (1953) 1069.
[2] G. Doucas, J.H. Mulvey, M. Omori, J. Walsh and M.F. Kimmitt, Phys. Rev. Lett. 69 (1992) 1761.
[3] J.P. Bachheimer, Phys. Rev. B 6 (1972) 2985.
[4] E.L. Burdette and G. Hughes, Phys. Rev. A 14 (1976) 1766.
[5] A. Gover, P. Dvorkis and U. Elisha, J. Opt. Soc. Am. B 1 (1984) 723.
[6] I. Shih, W.W. Salisbury, D.L. Masters and D.B. Chang, J. Opt. Soc. Am. B 7 (1990) 351.
[7] F.S. Rusin and G.D. Bogomolov, Proc. IEEE 57 (1969) 720.
[8] R.P. Leavitt, D.E. Wortman and C.A. Morrison, Appl. Phys. Lett. 35 (1979) 363.
[9] D.E. Wortman, R.P. Leavitt, H. Dropkin and C.A. Morrison, Phys. Rev. A 24 (1981) 1150.
[10] J.D. Jackson, Classical Electrodynamics (Wiley, New York, 1975) chap. 14, p. 671, Eq. 14 (70).
[11] G. Toraldo di Francia, Nuovo Cimento 16 (1960) 61.
[12] P.M. van den Berg, J. Opt. Soc. Am. 63 (1973) 1588.
[13] A. Gover and P. Sprangle, IEEE J. Quantum Electron. QE-17(7) (1981) 1196.
[14] L. Schachter and A. Ron, Phys. Rev. A 40 (1989) 876.
[15] K. Yasumoto, T. Tanaka and T. Aramaki, IEEE Trans. Plasma Sci. PS-18(4) (1990) 699.
[16] O. Haeberle, P. Rullhusen, J.-M. Salome and N. Maene, Phys. Rev. A, to be published.

Geometric approach to wavelength tuning of the Čerenkov free-electron laser

Emily E. Fisch and John E. Walsh

Department of Physics, Dartmouth College, Hanover, New Hampshire 03755-3528

Received January 30, 1992

We present a new and greatly simplified derivation of the tuning relation for a Čerenkov free-electron laser. The laser uses an electron beam to excite coherent light in a planar waveguide. The geometric (or zig-zag) theory of waveguides is used to model the set of guided modes, while properties of hte Čerenkov radiation dictate which modes are excited. The results obtained are identical to earlier research based on the formal application of Maxwell's equations. However, the geometric approach adds physical insight into the Čerenkov free-electron laser design problem. The dependence of output wavelength on electron-beam voltage and resonator thickness is plotted. A sample laser is designed for operation from 150 to 825 μm.

The Čerenkov free-electron laser (FEL) is an electron-beam-driven source of tunable, coherent radiation. It consists of an electron beam passing over a dielectric resonator and is shown schematically in Fig. 1. When the electron velocity is close to the phase velocity of light in the dielectric, energy is transferred from the electrons to a TM mode. (The TE mode is not excited because it has no axial electric field to exert a force in the direction of electron motion.) The electrons bunch in the retarding phase of the field and radiate coherently. For a given resonator, the electron energy dictates the wavelength of this coherent light. This tunability transforms the FEL from a laboratory curiosity to a potentially indispensable laboratory tool.

Wavelength tuning of the Čerenkov FEL has been demonstrated[1] and modeled. Past theoretical treatments[2] relied on a strict application of Maxwell's equations in the waveguide and vacuum regions. Boundary conditions were imposed to determine the dispersion relation, $D(\omega, k_z) = 0$. This function of the output frequency ω and the longitudinal wave number k_z must be solved numerically. The results may be displayed on the ω–k_z plane or rewritten in terms of measurable quantities such as wavelength and beam energy. The technique is time consuming, and little physical insight is gained. A simpler approach grows naturally from the geometrical-optics view of waveguides[3] and is presented in this Letter.

In the zig-zag theory of guided waves, a plane wave in the dielectric waveguide propagates through successive reflections at the dielectric–air interface. To apply this concept to the Čerenkov FEL, consider the planar slab resonator of thickness d and index n_1 suspended in vacuum ($n_2 = 1$). It is illustrated in Fig. 2. The modes of interest are guided TM modes. To remain within the dielectric, these modes must be incident at the air interface at an angle that exceeds the critical angle for total internal reflection, $\theta_{\text{crit}} = \sin^{-1}(n_2/n_1)$. In this limit the reflection coefficient $R = |r|^2 \exp(i2\delta)$ is complex with an amplitude of 1 and a phase shift given by[3]

$$\delta_{\text{TM}} = \tan^{-1}\left\{\frac{\left(\frac{n_1}{n_2}\right)^2\left[(n_1 \sin\theta_1)^2 - {n_2}^2\right]^{1/2}}{n_1 \cos\theta_1}\right\}. \quad (1)$$

The subscript TM is included to emphasize the polarization dependence of the equation. The wave must also be self-consistent: the sum of all the phase shifts in a round trip must be a multiple of 2π. In a round trip, the ray travels from $x = 0$ to $x = d$, is reflected at $x = d$, travels back from $x = d$ to $x = 0$, and is again reflected at $x = 0$. Adding these phase contributions gives the transverse resonance condition,

$$2\frac{\omega d}{c} n_1 \cos\theta_1 - 4\delta_{\text{TM}} = 2M\pi, \quad (2)$$

where $M = 0, 1, 2, \ldots$ is the mode number. Substitution of Eq. (1) into Eq. (2) and solving for the dimensionless frequency gives all possible values of $\omega d/c$ as a function of n_1 and θ_1:

$$\frac{\omega d}{c} = \frac{1}{n_1 \cos\theta_1} \times \left(M\pi + 2\tan^{-1}\left\{\frac{n_1}{\cos\theta_1}[(n_1 \sin\theta_1)^2 - 1]^{1/2}\right\}\right). \quad (3)$$

The information contained in this equation becomes apparent when the origin of the guided radiation in a Čerenkov FEL is considered.

All possible guided modes of the resonator are described by Eq. (3). We are concerned only with those that will be excited by an electron beam. A necessary condition for the interaction is that the electron is located within the evanescent tail of the mode. This evanescence length is quantified by refining the notion of reflection at an interface. The phase shift δ_{TM} may be treated as an increase in the ray's path length (the Goos–Hänschen shift) as shown in the detail of Fig. 2. At the interface the

0146-9592/92/110813-03$5.00/0

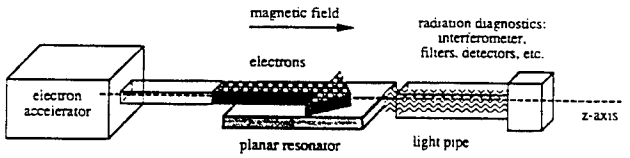

Fig. 1. Schematic view of the Čerenkov FEL. The presentation is intentionally vague because the design specifics (electron-beam voltage, resonator dimensions) are dictated by the chosen region of operation.

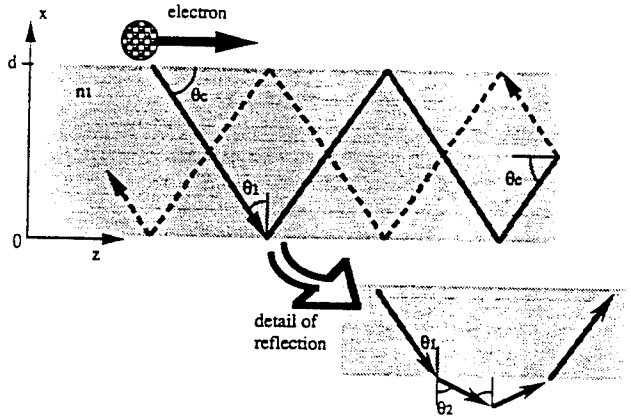

Fig. 2. Geometric view of guided modes in the Čerenkov FEL. A planar resonator of index n_1 and thickness d is suspended in vacuum. An electron beam propagates parallel to the surface of the resonator, along the z axis. A guided mode is represented by a ray that has total internal reflection at the dielectric–air interface. The angle of propagation is dictated by the angle of Čerenkov emission and is its complement. The detail illustrates the Goos–Hänchen shift. This is a geometric interpretation of the phase shift that occurs on reflection at an interface.

ray of magnitude $|\mathbf{k}| = \omega/c$ is refracted according to Snell's law and subsequently reflected at a virtual surface a short distance from the real one. The effective wave number representing the penetration into the vacuum is imaginary. With the use of trigonometric relations and Snell's law it can be written in terms of previously defined quantities:

$$iq = \frac{\omega}{c}(1 - n_1^2 \sin^2 \theta_1)^{1/2}. \tag{4}$$

The meaning of the imaginary q is that the plane wave's vacuum amplitude no longer oscillates but decays as $\exp(-qx)$, where x is measured from the interface. The mode maintains a reasonable amplitude within an evanescence length of $x = 1/q$.

Expressing quantities in terms of an arbitrary ray angle θ_1 is of limited value unless the directional nature of Čerenkov emission is incorporated. When an electron propagates along the z axis through the evanescent tail at a velocity $\beta = v/c > 1/n_1$, it creates an optical shock wave. The resulting light is emitted as a half-cone in the dielectric. It propagates at an angle to the z axis given by

$$\theta_c = \cos^{-1}\left(\frac{1}{\beta n_1}\right) \tag{5}$$

and known as the Čerenkov angle. The electron velocity and the index of the material dictate the angle of emission; it is larger for optically dense materials and fast electrons. This emission angle selects a particular resonator mode. θ_c is just the complement of θ_1, so Eq. (3) may be rewritten to accommodate the Čerenkov emission explicitly. By substituting $\sin \theta_1 = \cos \theta_c = 1/\beta n_1$ and $\cos \theta_1 = \sin \theta_c = [1 - (1/\beta n_1)^2]^{1/2}$, we can write

$$\frac{\omega d}{c} = \frac{\beta}{(n_1^2\beta^2 - 1)^{1/2}} \times \left(M\pi + 2\tan^{-1}\left\{n_1^2\left[\frac{1-\beta^2}{(n_1^2\beta^2-1)^{1/2}}\right]^{1/2}\right\}\right). \tag{6}$$

The excited frequencies are now specified entirely by the material index n_1, the electron velocity β, and a mode number M. The same expression can be extracted from the formal electromagnetic dispersion $D(\omega, k_z) = 0$ when synchronism ($\beta = \omega/ck_z$) is assumed and the necessary manipulations are performed. The relation itself is not new, but the intuitive application of geometric optics is presented here for what is to our knowledge the first time.

The above arguments may also be applied to evaluate the modes' vacuum penetration depth. Substituting Eq. (5) into Eq. (4), we can write q in terms of the electron energy $\gamma = (1 - \beta^2)^{-1/2}$, relative velocity β, and free-space wavelength $\lambda = 2\pi c/\omega$: $q = 2\pi/\lambda\beta\gamma$. The entire electron beam of thickness σ_b should be within a few evanescence lengths of the waveguide. Assuming that the beam just skims the dielectric surface, the restriction becomes

$$\frac{\sigma_b}{\lambda\beta\gamma} \approx 1. \tag{7}$$

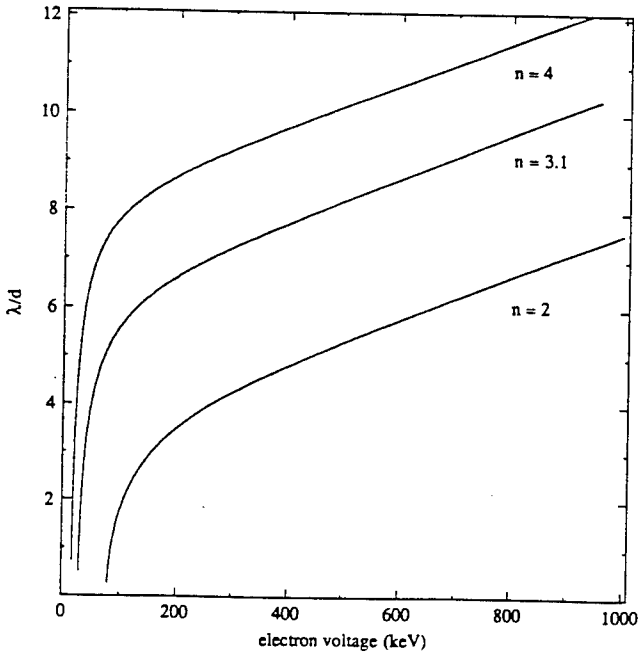

Fig. 3. Normalized wavelength λ/d plotted versus the electron-beam voltage for quartz, sapphire, and germanium planar resonators ($n_1 = 2$, 3.1, and 4, respectively) suspended in vacuum ($n_2 = 1$). The output wavelength is shorter at lower energies, where the steepest part of the tuning curve is found. There is no Čerenkov emission at voltages that do not accelerate the electrons to superluminal velocities. Higher-order modes are similar but are shifted to shorter wavelengths.

For practical design, a plot of the dimensionless wavelength $\lambda/d(n, \beta, M)$ as a function of electron-beam voltage $V(\beta)$ is useful. Equation (6) is easily rewritten in terms of the wavelength by noting that $\lambda/d = 2\pi/(\omega d/c)$. The electron accelerating voltage can also be expressed as a function of relative velocity β,

$$V(\text{keV}) = \left[\left(\frac{1}{1-\beta^2}\right)^{1/2} - 1\right]511. \quad (8)$$

Sample tuning plots for quartz, sapphire, and germanium planar resonators are shown in Fig. 3 for the TM_{01} mode.[4] Notice that no radiation is generated below a specific voltage. The threshold corresponds to the point at which electrons no longer exceed the speed of light in the medium c/n_1. Substituting the threshold velocity $\beta = 1/n_1$ into Eq. (8) gives an equation for the threshold voltage,

$$V_T(\text{keV}) = \left[\left(\frac{n_1^2}{n_1^2 - 1}\right)^{1/2} - 1\right]511. \quad (9)$$

The procedure for designing a practical source of radiation to operate in a specific spectral region is straightforward. The sapphire planar slab resonator has produced radiation in our laboratory[5] and will be used as an example. Our accelerator produces 20–100-keV electrons. The threshold voltage for sapphire ($n_1 = 3.1$) is calculated from Eq. (9) to be 29 keV. The appropriate curve on Fig. 3. indicates that 29–100 keV corresponds to $\lambda/d =$ 1–5.5. Assume that we choose to operate in the far-infrared region of the spectrum, 100 μm to 1 mm. This is a logical choice since there are few comparable sources there. A planar slab 150 μm thick would tune from $\lambda = 150$ to 825 μm, an astonishingly broad range. Perhaps the most difficult aspect of the design (when presented in this manner) is choosing a material that maintains the appropriate index and sufficiently low absorption throughout the target spectral region.

The support of Vermont Photonics, Inc., and U.S. Army Research Office contract DAALO3 91-G-0189 is gratefully acknowledged.

References

1. E. Fisch and J. Walsh, Appl. Phys. Lett. **60**, 129 (1992).
2. J. E. Walsh, in *Laser Handbook*, W. B. Colson, C. Pellegrini, and A. Renieri, eds. (Elsevier, Amsterdam, 1990), Vol. 6, p. 485 and references therein.
3. H. Kogelnik, in *Integrated Optics*, T. Tamir, ed. (Springer-Verlag, Berlin, 1975), pp. 15–79.
4. The standard convention for mode labeling is employed: the first index refers to the number of half wavelength variations in y (width), and the second index refers to the variations in x (height). Since the derivation imposed no restrictions on the width, this first index must be zero.
5. We do not include the details of FEL gain and its impact on the resonator length and electron-beam parameters (current density, energy spread). Such considerations are beyond the scope of this Letter and have little impact on the wavelength tuning. They are, however, essential to the design of a feasible laser source.

First Observation of Smith-Purcell Radiation from Relativistic Electrons

G. Doucas, J. H. Mulvey, and M. Omori
Department of Physics, Oxford University, Oxford, England

J. Walsh
Department of Physics, Dartmouth College, Hanover, New Hampshire 03755-3528

M. F. Kimmitt
Department of Physics, Essex University, Colchester, Essex, England
(Received 26 May 1992)

A beam of 3.6-MeV electrons has been used to study the generation of radiation in the far infrared (FIR) by the Smith-Purcell mechanism. The dependence of wavelength on angle of emission, over angles from 56° to 150° and wavelengths from 350 to 1860 μm, is in excellent agreement with the Smith-Purcell dispersion relation. Comparison of the yield with that from a 5000-K source suggests that the spontaneous Smith-Purcell effect offers an easily tunable alternative to the synchrotron as a coherent FIR source, and that it could also form the basis of an inexpensive, compact free-electron laser.

PACS numbers: 41.75.Ht, 41.60.Cr

We report the first observations of Smith-Purcell (SP) radiation in the submillimeter–far-infrared region of the spectrum. Unlike both early [1] and more recent work [2], which relied on low-energy electron beams and concentrated on emission in the visible, here a relativistic electron beam was employed and the emphasis is on a spectral region where the population of sources is sparse.

Comparison of the measured value of the emitted wavelength (λ_{SP}) and the emission angle (θ) for a series of gratings confirms in detail that the process obeys the celebrated SP formula:

$$\lambda_{SP} = \lambda_G [1/\beta - \cos\theta] . \quad (1)$$

The parameter λ_G is the grating period and β is the relative velocity of a beam electron. In the spectral region where the radiation was observed, the level is comparable to that produced by an infrared beam line on a synchrotron. The emission from compact, linear-accelerator-driven gratings would be much greater. Thus, the process provides a means whereby Fourier-transform spectroscopic techniques can be extended into the technologically important long-wavelength spectral region. The grating is also a much simpler structure than a magnetic undulator and with adequate feedback it offers another basis for the free-electron laser (FEL) [3].

The inverse SP process has also been considered as a possible means of accelerating electrons to high energy [4]. Although in the present work acceleration was not the object, coupling of near speed of light electrons and gratings has been demonstrated.

The electrons were accelerated in a modified 10-MV Van de Graaff accelerator formerly used for a program of nuclear structure research at Oxford. Conversion to accelerate electrons had been started in preparation for a FEL project which was then not funded. Work necessary to enable efficient electron transmission [5] was completed and an electron gun was kindly lent by the Department of Physics, University of Glasgow.

First, acceleration of the electrons was obtained at an energy of 3.6 MeV. The grid of the gun was pulsed, giving 6-μs bursts of electrons at 1 Hz. Considerable difficulties were experienced with both the yield and short lifetime of the cathodes; these were not fully overcome. Another pair of unsolved problems were a slight positional jitter in the beam and a beam size slightly larger than expected. The beam size, shape, and transverse position could be controlled using the up-stream deflecting magnets and quadrupole (Fig. 1).

The electron beam current was measured at the gun exit and by measuring the charge collected on the grating and the beam dump; the latter signal also served as a trigger for recording the Smith-Purcell optical signal. The data were taken with a beam size which was 3 mm (normal to the grating) by 6 mm (transverse), and beam currents varied from 50 mA up to a maximum of 200 mA, giving current densities in the range of 0.35 to 1.7 A/cm^2.

The arrangement for the observation of Smith-Purcell

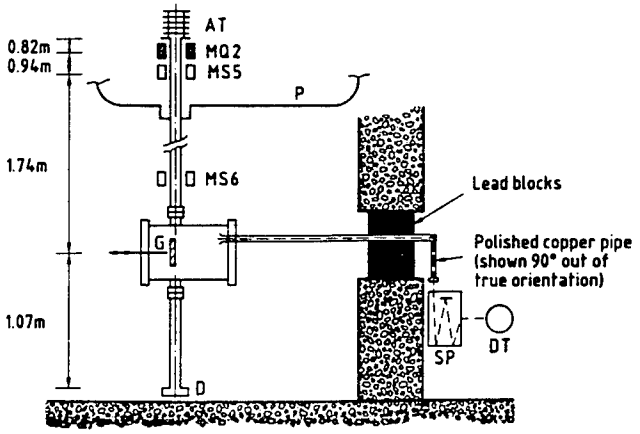

FIG. 1. Schematic of the experiment layout showing beam control elements, grating and optical chamber, light pipe, x-ray shielding, spectrometer, and detector.

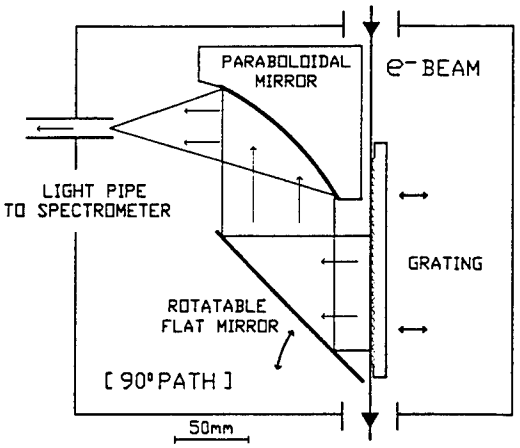

FIG. 2. Diagram illustrating the optical arrangement. Rotation of the flat mirror allows observation of radiation emitted from the grating at angles from 25° to 94° to the forward beam direction. By turning the optical platform through 180°, emission angles of 85° to 155° could be studied.

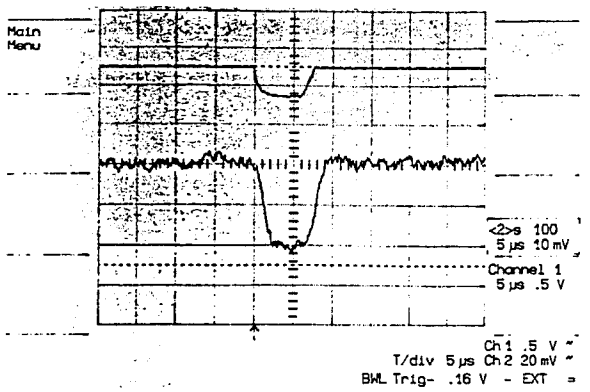

FIG. 3. A typical Smith-Purcell signal, averaged over 100 pulses and recorded on a Lecroy 9400A digital oscilloscope; upper trace is the electron beam pulse, used as a trigger.

radiation is illustrated in Figs. 1 and 2. In order to detect the radiation emitted over a range of angles, a rotatable plane mirror from which the light collected was focused at the entrance of a 2-m-long internally polished copper tube. This took the light to the entrance of a Czerny-Turner spectrometer behind a lead-brick wall.

A helium-cooled InSb electron bolometer was placed at the exit slit of the monochromator. This had a response time of ~ 0.5 μs and could detect peak powers of less than 10 nW over the wavelength range 400–2500 μm.

The light pipe was evacuated separately from the accelerator and beam transport, with TPX windows at both ends and a third at the cryostat entrance. The air path in the spectrometer was about 4 m.

Movement of the plane mirror enabled observations at emission angles of 25° up to 94° from the forward direction of the beam. The relationship between mirror angle and emission angle was directly calibrated externally using a helium neon laser. Angles in the backward direction could be reached by dismounting the plate carrying the grating and mirrors, rotating it through 180°, and introducing a short periscope to convey the light to the light pipe entrance. It was subsequently discovered that a slight misalignment occurred in the periscope and a 2° correction was applied to this set of data. The positions of the plane mirror and the grating were under independent remote control, as was the angle of the spectrometer grating.

The gratings were ruled with a 30° blaze on aluminum bars 2 cm in width, with a slightly concave surface facing the beam, and with an effective optical length of about 7 cm along the beam.

A typical Smith-Purcell signal, as recorded on the Lecroy model 9400A digital oscilloscope averaged over 100 pulses, is shown in Fig. 3. This was obtained with a 3.6-MeV electron beam passing over a (nominal) 0.030-in. period grating; the emission angle was 136° and the wavelength 1300 μm. Figure 4 shows the signal as a function of wavelength in another case using the same grating at an emission angle of 115°. The FWHM is about 88 μm, consistent with the range of efficient collection in angle of the optical system and wider than the spectrometer bandwidth.

The results obtained in two runs are summarized in the plot (Fig. 5) of observed wavelengths, λ_{obs}, against the values predicted from the dispersion formula (1), λ_{SP}. The agreement is excellent over the whole range [6] of angles explored, from 56° to 150°. There can be no doubt that this is Smith-Purcell radiation.

Subsequently the grating was replaced by a high-pressure mercury vapor lamp with an arc temperature of ~ 5000 K above 400 μm [7]. This allowed a direct calibration of the entire system, using the same optical train, spectrometer, and detector. The preliminary analysis of the results, Fig. 6, shows the yield of Smith-Purcell radiation generated by a 0.1-A electron beam and entering the detector to be greater than that from the mercury source for wavelengths above 600 μm, and more than 10 times

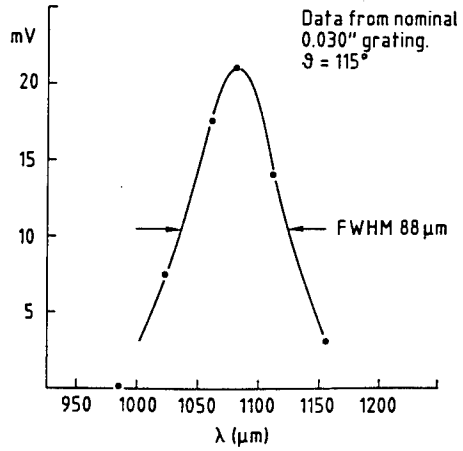

FIG. 4. Smith-Purcell signal as a function of wavelength, for emission angle of 115° from nominal 0.030-in. period grating.

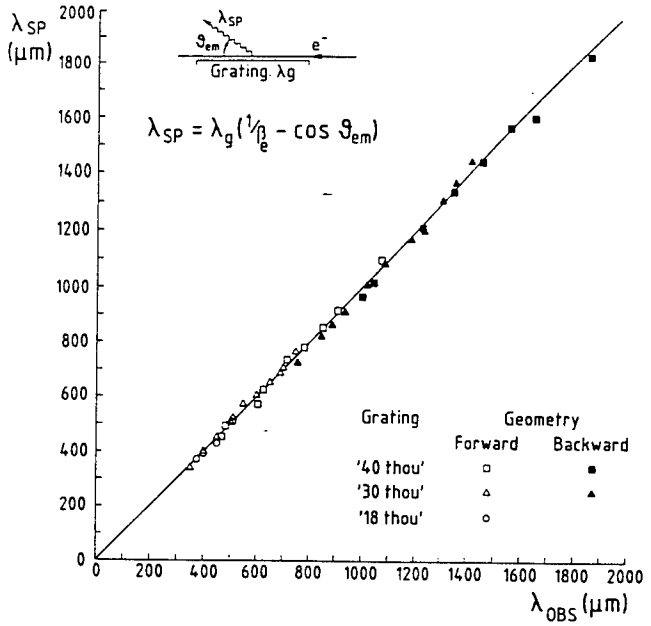

'FIG. 5. Predicted Smith-Purcell wavelength, λ_{SP}, vs the observed wavelength, λ_{obs}, for the conditions indicated. The wavelengths covered by one grating (nominal 0.40-in. period) range from 467 to 1860 μm.

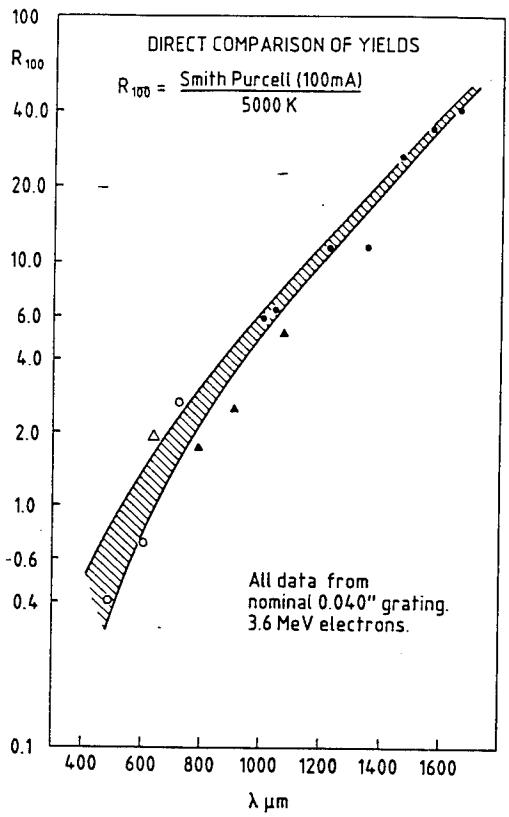

FIG. 6. A direct comparison as a function of wavelength of the Smith-Purcell signal levels form a 0.040-in. grating with those obtained from a 5000-K source under closely similar conditions.

larger for wavelengths greater than 1200 μm. Figure 6 uses data from four different runs and the systematic shifts in position are consistent with being due to difficulties in reproducing identical operating conditions for the beam; however, the overall conclusion is not affected.

It is also instructive to compare the power levels observed with the performance of an infrared beam line on a synchrotron [8]. Following Ref. [8] we observe that the National Synchrotron Light Source beam produces approximately 10^{16} photons/secsr in a 0.1% bandwidth at a wavelength of 1 mm for a current of 1 A. The present SP source produces approximately 10^{15} photons/secsr in the same fractional bandwidth when the current is 100 mA. Thus, these sources are comparable at this wavelength.

Detailed theoretical models of the emission process have not yet been subjected to any critical experimental test; however, assuming that the SP process falls in the general category of wake field phenomena [3], emission should scale as

$$\frac{dP}{dz} \sim A_b e^{-\lambda_0/\lambda} \frac{d\lambda}{\lambda^3}, \tag{2}$$

where A_b is of the order of the beam area and the exponential term results from the coupling to the space harmonic component whose phase velocity is synchronous with the beam velocity. The characteristic cutoff wave number λ_0 will scale [3] with $\bar{\sigma}/\beta\gamma$ where $\bar{\sigma}$ is the beam thickness and γ is the relative energy. In the present experiment $\bar{\sigma}$ was approximately 2 mm and the estimated beam emittance was very high ($> 20\pi$ mm mrad, normalized). A low-emittance, low-energy, compact linear accelerator will, on the other hand, have a typical emittance in the $4-5\pi$ mm mrad range in the energy range of these experiments. Thus, $\bar{\sigma}$ in the 0.2–0.4-mm range are easily obtained. The linac will also have much higher (peak) current. In the best case a micropulse may contain 1–2 nC of charge and hence $I_b \sim 100$ A is available. The radiation produced by a grating driven by such a beam would exceed the level produced by a synchrotron (and a blackbody) by many orders of magnitude.

Smith-Purcell radiation has been observed in the far infrared generated by relativistic electrons of energy 3.6 MeV, over a continuous range of emission angles from 56° to 150°, and wavelengths from 350 to 1860 μm.

The first indications from a direct calibration using a mercury vapor source at ~5000 K are that even with an electron beam clearly very inferior to state of the art, the yield can be significantly greater in this region of the spectrum and, given optimal beam conditions, suggest that a device based on the spontaneous Smith-Purcell mechanism could rival the synchrotron as a coherent FIR source.

Moreover, these results give encouragement to proposals to use the Smith-Purcell effect as a basis for an inexpensive, compact, easily tunable ir FEL [3].

The Oxford group wishes to thank their colleagues in the Particle and Nuclear Physics Laboratory for their support of this experiment, especially in times of great

pressure on resources. We also thank Professor Bob Owens of Glasgow University for the loan of an electron gun. The successful conversion and operation of the Van de Graaff for this last experiment was made possible by the enthusiasm and efforts of Tony Henwood, Colin Graham, George Hammett, and Bill Linford who also designed and made the grating and optics mounting; finally we thank Brian Hawes and Graham Salmon for their help and advice on the cryogenics. EC European Network Contract [SC1-0471-C (A)] provided funds for certain travel expenses, and for the purchase of the InSb crystal lent by Professor Carl Pidgeon of Heriot Watt University. J.W. wishes to acknowledge support from Vermont Photonics, Inc., from U.S. ARO Contract No. DAAL03-91-G-0189, and from NSF Contract No. INT-8815235.

[1] S. J. Smith and E. M. Purcell, Phys. Rev. **92**, 1069 (1953).

[2] W. W. Salisbury, Science **154**, 386 (1966); J.-P. Bachheimer and J.-L. Bret, C. R. Acad. Sci. Paris **266**, 902 (1968); J.-P. Bachheimer, Phys. Rev. B **6**, 2985 (1972); A. Gover and Z. Livni, Opt. Commun. **26**, 375 (1978); A. Gover, P. Dvorkis, and U. Elisha, J. Opt. Soc. Am. B **1**, 723 (1984).

[3] J. Walsh and E. Fisch, in *Proceedings of the 1991 Free-Electron Laser Conference* [Nucl. Instrum. Methods Phys. Res., Sect. A **318**, 772 (1992)]; E. Price and J. Walsh, Appl. Phys. Lett. (to be published).

[4] R. B. Palmer, Particle Accel. **11**, 81–90 (1980).

[5] G. Doucas, J. H. Mulvey, and M. Omori, in Proceedings of the Sixth International Conference on Electrostatic Accelerators and Associated Boosters, Montegrotto Terme, Padova, Italy, 1–5 June 1992 (to be published).

[6] With the gratings used, at angles forward of 56°, the wavelength drops below about 350 μm where the detector sensitivity is falling rapidly.

[7] M. F. Kimmitt, *Far Infrared Techniques* (Pion Ltd., London, 1970), p. 51.

[8] G. P. Williams, Nucl. Instrum. Methods Phys. Res., Sect. A **291**, 8 (1991).

Operation of the sapphire Cerenkov laser

E. E. Fisch and J. E. Walsh
Department of Physics, Dartmouth College, Hanover, New Hampshire 03755

(Received 15 November 1991; accepted for publication 20 January 1992)

First operation of a sapphire-based Cerenkov free electron laser is reported. It is a tunable source of coherent millimeter and submillimeter radiation. The phase velocity of light in sapphire is about one-tenth of that in free space so that Cerenkov radiation is obtained at modest electron beam energies. In addition to its role as a Cerenkov coupler, the sapphire forms a high Q resonator obviating external mirrors. The spontaneous Cerenkov emission is well-confined by this resonator and can build to watts of power. Measured tuning and threshold currents are presented and compared with the predictions of free electron laser theory.

Although similar to earlier Cerenkov free electron lasers (CFELs),[1] the sapphire-based Cerenkov laser is unequivocally novel. The inherent advantages of wiggler-type FELs are retained: the radiation is tunable, coherent, and useful levels of power are produced. Additional advantages are introduced by the sapphire resonator. The coupling between the free electrons and the optical wave is achieved via the sapphire resonator obviating the need for a complicated magnetic wiggler. Sapphire has been widely studied for applications as a window, substrate, or laser host material. Consequently, its properties are well-characterized. Sapphire is also convenient to use; it is durable, chemically inert, available, and inexpensive.

The dielectric serves two functions. It slows the phase velocity of the radiation so that Cerenkov emission is possible and contains this radiation in discrete resonator modes. Only the TM modes are excited because the longitudinal E field is required to couple to the electron beam. The TM field components are harmonic solutions to Maxwell's equations. Imposing the continuity of the fields at interfaces yields a dispersion relation whose form depends on the resonator geometry. Synchronism between the optical mode's relative phase velocity ω/ck_z and the electron velocity β is required for efficient beam/mode coupling. When synchronism is imposed on the dispersion relation, the free-space output frequency ω as a function of β is obtained. For a dielectric film of thickness d and index n on a metal substrate it is

$$\left(\frac{\omega d}{c}\right)_{\text{film}}=\frac{\beta}{\sqrt{\beta^2n^2-1}}\tan^{-1}\left(n^2\sqrt{\frac{1-\beta^2}{\beta^2n^2-1}}\right). \quad (1)$$

This expression describes the fundamental TM mode. Higher order modes are obtained by realizing that $\tan^{-1}(x)=\tan^{-1}(m\pi+x)$ where $m=0,1,2,\ldots$. A slab (no metal substrate) of the same thickness would generate twice the frequency predicted by Eq. (1) in its lowest order asymmetric mode.

The gain of the device is calculated using the dimensionless FEL laser variables and equations presented in Brau's book on free-electron lasers[2] and in many of Colson's papers.[3] Time is normalized to the resonator transit time of an electron, $\tau=\beta ct/L$ where the electron's velocity is βc and L is the length of the resonator. For a given electron, τ is 0 at the beginning of the resonator and 1 at the end. The relative electron phase $\zeta=k_z z(t)-\omega t$ is inherently dimensionless. The change in ζ with respect to τ defines a velocity-like variable ν. Using a dimensionless field amplitude ϵ with the position and velocity coordinates, the pendulum equation of motion for the system is written

$$\frac{d^2\zeta}{d\tau^2}=\frac{d\nu}{d\tau}=-\epsilon\sin(\zeta). \quad (2)$$

It is one of two equations which determine the behavior of the FEL. The other is the wave equation. For a spatially uniform (dimensionless) electric field, it is

$$\frac{d\epsilon}{d\tau}=-j_e\,[\sin(\zeta)]. \quad (3)$$

j_e is the dimensionless electron current. It determines how strongly the field amplitude and optical phase are driven. Modeling the laser in terms of Eqs. (2) and (3) yields an expression for the current. For the dielectric film on a metal substrate, j_e is

$$j_e=\frac{L^3}{2d\sigma_x\sigma_y}\frac{I_e}{I_0}\frac{\omega d/c}{\beta_e^4\gamma_e^5}\frac{n^2\beta^2-1}{n^2-1}\left\{1+\frac{\omega d/c}{\beta_e\gamma_e}\left(1+\frac{n^2}{\gamma^2}\right)\right\}^{-1}f_c, \quad (4)$$

where $I_0=\epsilon_0mc^3/e=1356$ A is the fundamental current, σ_x and σ_y are the dimensions of the electron beam, and f_c is the coupling factor. f_c quantifies the spatial overlap between the electron beam and the optical mode. For an uncovered film it is

$$f_c=e^{-2q\delta}(1-e^{-2q\sigma_x}), \quad (5)$$

where δ is the gap between the dielectric surface and the electron beam. The expression is slightly more complicated when a ceiling plate is placed a distance b above the dielectric:

$$f_c=\frac{1}{\sinh^2 qb}\left[\sinh q\sigma_x\cosh 2q\left(b-\delta-\frac{\sigma_x}{2}\right)-q\sigma_x\right]. \quad (6)$$

This is the only difference in gain for the two geometries at energies less than about 5 MeV. The ceiling plate forces the field above the dielectric (where coupling occurs) into a

 0003-6951/92/111298-03$03.00

smaller region. A larger optical energy density is then available to interact with the finite electron beam. Hence, the coupling and gain improve for lower ceiling heights.

The FELs operating regime may be identified according to the magnitude of j_e : $j_e \ll 1$ is considered low gain and $j_e \gg 1$ is considered high gain. The sapphire laser is operating in the second limit where the gain is given by[3]

$$G=\frac{1}{9}\exp\left[3^{1/2}\left(\frac{j_e}{2}\right)^{1/3}\right]. \tag{7}$$

Lasing threshold occurs when the resonator losses are just compensated by the gain from the electrons, $G=\omega t_c/Q$ where t_c is the electron transit time, $L/\beta c$, and Q is the quality of the resonator. It is useful to solve for the threshold current

$$I_{\text{th}}=\frac{2I_e}{j_e}\left[3^{-3/2}\ln\left(9\frac{\omega L}{c\beta_e}\frac{1}{Q}\right)\right]^3, \tag{8}$$

because it can be measured experimentally. I_e appears explicitly, precisely because it must be divided out of the expression for j_e, not because it is a factor.

An expression for Q is needed. The resonator of interest is just the dielectric of length L and thickness d. Its quality is not constant, but is easily modeled in terms of the standard expression

$$Q=\frac{\omega d/c}{\beta_g[2\alpha d-(d/L)\ln(R)]}. \tag{9}$$

Equation (1) is used to determine ω and β_g (the group velocity $d\omega/dk$). α is the material loss which can be found in the literature.[4] R is the intensity reflection coefficient at the end mirrors formed by the air/dielectric interface. Since Cerenkov emission occurs at an angle to the electron beam, $\theta_c=\cos^{-1}(1/\beta n)$, guided modes are incident at the end mirrors at θ_c and the Fresnel reflection coefficient can be calculated. Both Q, and hence the threshold current of Eq. (8), can be evaluated to characterize the sapphire CFELs operation.

The laser consists of two main parts: the electron beam (and associated hardware)[5] and the sapphire resonator. A Pierce-type gun produces 20–100 keV electrons which are collimated by a 6 kG dc axial solenoidal field. The resonator is located in the center of the solenoid so that an essentially one-dimensional electron beam travels along the resonator axis (z axis). The electrons are dumped after they traverse the resonator and the radiation is coupled out in a WR-28 rectangular waveguide. 1N53a diodes are used to detect radiation at frequencies below about 120 GHz. Higher frequencies are detected with a He-cooled InSb crystal.

Sapphire (Al_2O_3) is a uniaxial crystal with two indices of refraction corresponding to ordinary and extraordinary waves. Electron-beam propagation parallel to the c-axis generates a single symmetrical Cerenkov cone. Any other orientation would generate two cones and hence less-effective radiation production. As long as $c\|z$, the theory may assume an isotropic dielectric constant[4] $n_0=n=3.1$.

Data are presented for a sapphire resonator with dimensions $4.5\times1.5\times0.025$ in. ($114\times12.7\times0.635$ mm). It

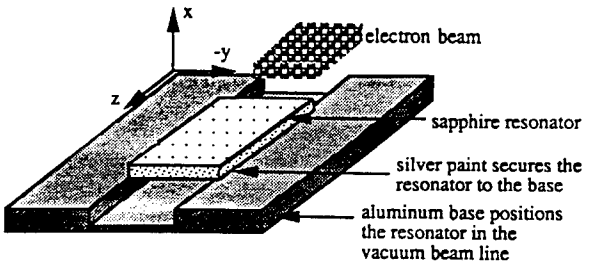

FIG. 1. A schematic view of the sapphire resonator as it is positioned in the experiments is shown. The crystal c-axis is parallel to the electron beam's velocity (both are in the z-direction). The resonator is usually covered with a flat aluminum plate in the yz-plane, a distance b above the dielectric surface.

is composed of three 1.5 in. long "slides" placed end-to-end. At mm wavelengths the discontinuity is insignificant. The slides (obtained from Meller Optics, Inc.) were optically polished to 10λ at 0.63 μm. They were fixed in the beam line with silver paint on the two long edges. Only these edges touched metal because of a trough below. The sapphire slab was, for calculational purposes, suspended in vacuum. A schematic of the resonator is shown in Fig. 1.

The electron voltage is related to the relativistic velocity β:

$$V[\text{keV}]=\left(\sqrt{\frac{1}{1-\beta^2}}-1\right)511. \tag{10}$$

All theoretical parameters may be plotted versus the laboratory quantity V rather than β. Sapphire's index and thickness determine the output frequency according to Eq. (1). This is plotted versus V in Fig. 2 with experimental data points. The frequency data were taken with a series of high-pass filters in front of the diode detector. The electron voltage was increased until no optical signal passed. This final V and the filter's frequency cutoff formed a data pair.

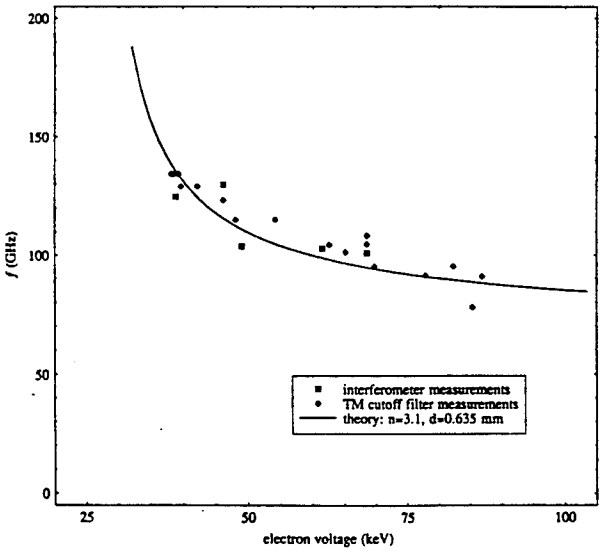

FIG. 2. Michelson interferometer and high-pass filter frequency measurements are plotted vs electron voltage (energy). The resonator was a sapphire slab $114\times12.7\times0.635$ mm. The theoretical tuning curve for the lowest order asymmetric TM mode is shown to fit the data well.

A Michelson interferometer was used to corroborate the data. It has the advantage of showing the spectral content, but is experimentally more difficult to use than filters. The interferograms showed the laser was single moded. The close correlation between the data and the tuning curve indicates that this excited mode was the lowest asymmetric TM mode.

The best way to verify the gain calculation is to find the lasing threshold where the gain is just sufficient to overcome the resonator loss and loading. Threshold current data were taken by maintaining a constant electron voltage and reducing the current until the optical signal could no longer be detected. The current was then turned back up until the signal returned. Occasionally the device needed slightly more current to turn on than off. The data shown in Fig. 3 are an average of the on and off currents taken with two ceiling heights. Trends for the two different ceiling heights (b's) indicate that the gain is higher for the smaller ceiling height as expected. For a given amount of total current the best way to drive the laser would be to have a very small b and a large current density.

The effect of sapphire thickness has also been examined. Equation (1) shows that the output frequency-dielectric thickness product is constant at a given β. This relation has been verified experimentally: about 200 GHz was produced with a single $1.5\times0.5\times0.010$ in. piece of sapphire at 80 keV. This gives virtually the same frequency-thickness product as was obtained with the thicker sapphire resonator plotted on Fig. 2. Shorter sapphire resonators have also been used. Lasing was achieved with two $1.5\times1.5\times0.025$ in. slides, but not with one. This is not surprising since gain increases exponentially with L [Eqs. (4) and (7)]. It should be emphasized that the critical quantity is not L, but L/d. The successful operation of the 1.5 in. long (one slide), 0.010 in. thick sapphire supports this assertion.

Scaling this device to operate in the source-poor far-infrared (1 mm–100 μm) should be straightforward. Phonon absorption between 5 and 200 μm should be avoided, but otherwise the optical properties of sapphire are excellent. Updating our beam technology would transform this sapphire CFEL into an extremely compact device. The simplicity of the sapphire planar resonator makes it a viable radiation source for a number of applications.

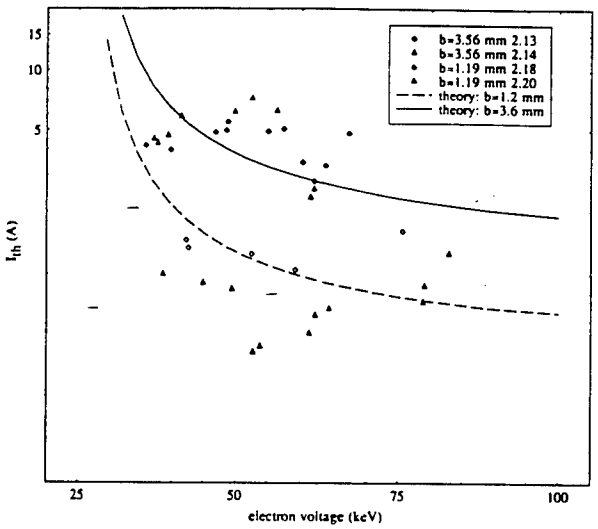

FIG. 3. The threshold current for two different ceiling heights ($b = 3.6$ and 1.2 mm) are plotted vs electron voltage. The resonators were otherwise identical sapphire slabs $114\times12.7\times0.635$ mm. Open symbols represent data taken with $b = 1.19$ mm and closed symbols represent data taken with $b = 3.56$ mm. The solid lines are theoretical predictions calculated from Eq. (8). The expected decrease in I_{th} (or equivalently increase in gain) with decreased b is clearly shown.

The support of Vermont Photonics, Inc. and USARO Contract No. DAALO3 91-G-0189 is gratefully acknowledged.

[1] J. E. Walsh, in *Laser Handbook*, edited by W. B. Colson, C. Pelligrini, and A. Renieri (Elsevier, Amsterdam, 1990), Vol. 6, p. 485, and references.
[2] C. A. Brau, *Free-Electron Lasers* (Academic, San Diego, CA, 1990).
[3] W. B. Colson and J. Blau, Nucl. Instrum. Methods **272A**, 386 (1988).
[4] E. V. Loewenstein, D. R. Smith, and R. L. Morgan, Appl. Opt. **12**, 398 (1973).
[5] K. L. Felch, Ph.D. thesis, Dartmouth College, 1980.

Operation of the grating-coupled oscillator at submillimeter/far-infrared wavelengths

E. J. Price and J. E. Walsh
Department of Physics and Astronomy, Dartmouth College, Hanover, New Hampshire 03755

(Received 22 November 1991; accepted for publication 21 May 1992)

Grating-coupled oscillator experiments covering the 1 cm–400 μm wavelength range are reported. Two coexisting modes of operation have been identified; a relatively low frequency signal (LFM) that is widely tunable with voltage and a high frequency signal (HFM) that tunes over a more reduced wavelength and voltage range. Observed wavelength and start oscillation currents of the LFM correspond well with a simple model of the beam-electromagnetic wave interaction. Electronic tuning ranges of 50 GHz with start oscillation currents of 0.5–1.5 A at beam voltages of 50–100 kV are typical. Power levels approach a kW at longer millimeter wavelengths.

It has been known since the early 1950's that the juxtaposition of a conducting metal grating and an electron beam can result in the production of radiation.[1] Many subsequent grating-based experiments have been performed in which spontaneous and stimulated radiation has been produced over a wide spectral range.[2–6] This letter is concerned with the development of a grating-coupled oscillator (GCO) radiation source in the submillimeter/far-infrared (FIR) regions of the spectrum. Prior experiments established the GCO as a viable source of coherent, tunable radiation at centimeter wavelengths.[7] Recent experiments have extended the operating wavelength to 400 μm.

The GCO is a metal-grating-based radiation source that exploits the interaction between electromagnetic fields supported by the grating structure and an electron beam skimming above the grating surface. The fields supported by the grating produce a current modulation and power is generated by stimulated emission. This occurs as a result of the interaction between the electron beam and an axial component of the electric field. The beam couples synchronously to space harmonic components of this field that possess phase velocities slightly slower than that of the electrons. Confocal mirrors placed at each end of the resonator are matched to the radiation distribution and provide feedback in a stable Gaussian pattern.

The operating wavelength of the device is determined by the accelerating voltage and the dispersion relation of the bound and radiating modes which exist above the grating. The dispersion relation is a universal self-similar function of the grating dimensions and is a periodic function of the guide wavenumber k. In general, it takes the form of $D(\omega\,\ell/c, k\ell)=0$ where ℓ is the grating period. Its detailed form is dependent upon the choice of grating geometry but the general features follow simply from periodicity. Making the approximation that beam-wave synchronism occurs when the phase velocities of the beam and wave are equal allows for an electronic tuning curve to be generated from the dispersion relation.

In addition to the dispersion and electronic tuning, the GCO can be further characterized by a calculation of the gain, which determines the start oscillation current limits of the various modes. The gain of the device can be written (in the low current density limit) as

$$\Omega = -\frac{1}{\epsilon_t} d\epsilon/dt$$

where ϵ_t is the total electromagnetic energy stored in the resonator and $d\epsilon/dt$ is the energy that is interchanged between the electromagnetic fields and the electron beam. If the major source of loss in the cavity is assumed to be due to the mirrors, then a simple expression for the amount of current needed to initiate oscillation can be obtained, given by

$$I_{st} = \left(\frac{cI_b}{L\Omega}\right) \ln \sqrt{R_1 R_2}.$$

I_b is the beam current and effectively sets that beam density, L is the resonator length and R_1, R_2 are the mirror reflectivities. The start oscillation current can be measured and compared directly with this prediction.

A series of experiments have been carried out to test the theoretical predictions and to extend the operating wavelength of the GCO to the FIR. A schematic of the experimental apparatus is shown in Fig. 1. A tungsten cathode coated with barium oxide supplies current at accelerating voltages up to 150 keV. The resonator structure is situated in the center of the magnetic field that serves to guide the beam along the grating. A perspective view of the resonator is shown in Fig. 2. The grating is located in the center of a confocal cavity with input–output apertures in the mirrors that allow for transmission of the beam

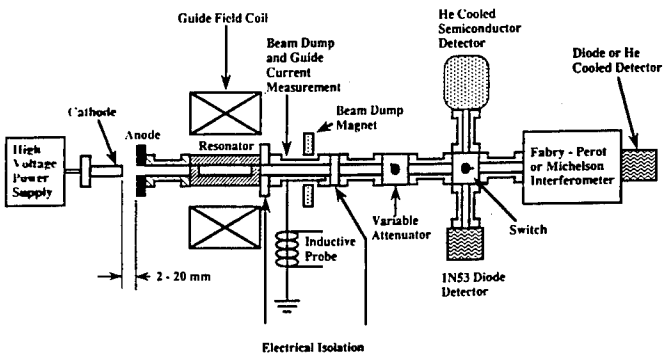

FIG. 1. A schematic view of the experimental apparatus is shown in block form.

 0003-6951/92/280252-03$03.00

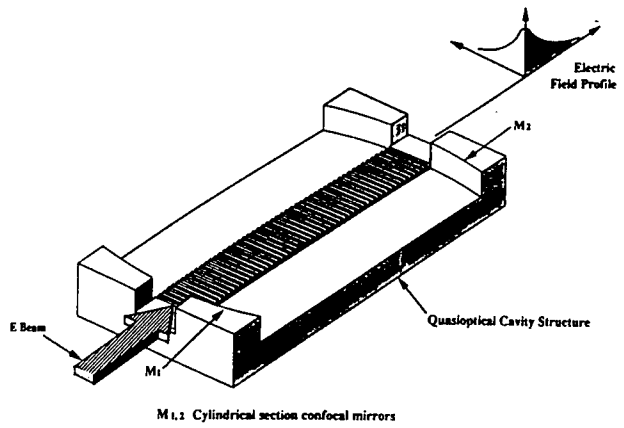

FIG. 2. A perspective view of the grating resonator system is shown. The grating profile shown is rectangular; the data presented herein were obtained with triangular grating profiles.

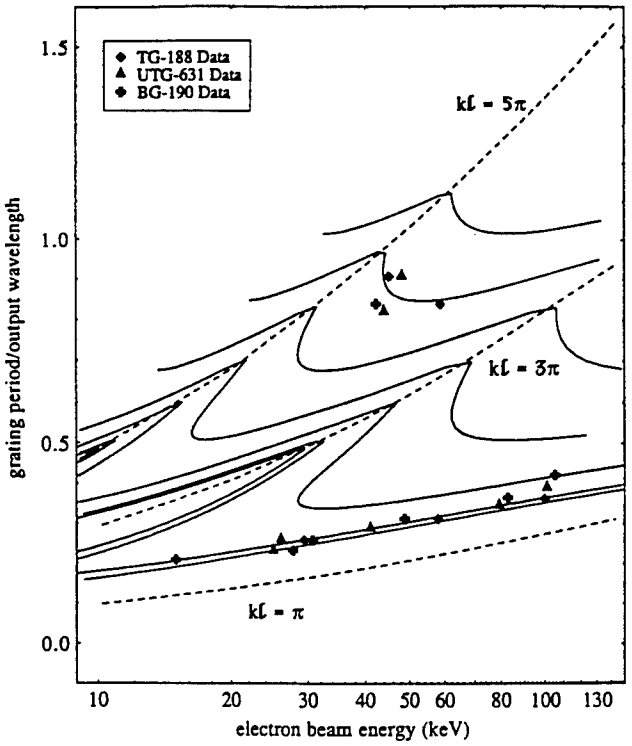

FIG. 3. Electronic tuning curves are shown with both HFM and LFM data. The dashed lines represent constant values of $k\ell$. If the dashed lines were mapped onto the periodic dispersion plane, each would bisect a Brillioun zone.

through the system as well as extraction of the radiation. Radiation is coupled out using WR-28 waveguide and an array of diagnostics are used to analyze the radiation. Detection of the radiation is accomplished using either semiconductor detector diodes or liquid helium-cooled bolometers. Calibration of the detectors for power measurements is achieved using Gunn diodes and a CO_2 pumped FIR laser. Wavelength diagnostics include high-pass filters and various interferometers.

The output wavelength, power, and start oscillation current are determined as a function of the electron beam energy for a number of different gratings. The initial experiment that utilized a triangular grating geometry resulted in LFM operation over the range 39–69 GHz and HFM operation over the 148–173 GHz range. Figure 3 shows the theoretical predictions for the electronic tuning for several modes along with typical LFM and HFM tuning data for several gratings. In the example shown, the LFM interaction occurs in the first Brillioun zone (i.e., in the region $\pi \leqslant k\ell \leqslant 2\pi$). The HFM operates in the second zone with $k\ell \approx 4\pi$. The location of the operation of the HFM has been seen to depend strongly on the ratio of the channel height to the grating period, so only those cases that have the same ratio are plotted together. To further identify the mode responsible for LFM operation, measurements of the start oscillation current were performed and compared with theoretical predictions. The start current as a function of the accelerating voltage is shown in Fig. 4 for UTG-631.

In order to establish the scaling of the output wavelength with grating parameters, a number of different gratings have been utilized. All of these gratings possess a triangular geometry. Experiments aimed at short wavelength

TABLE I. Compilation of experiments.

Grating name	Grating period (mm)	Grating width (mm)	Grating angle (deg)	Tuning range (GHz)	Beam energy range (keV)
TG-188	1.57	20.2	60	40–69	27–100
				148–173	44–59
BG-190	1.57	20.2	45	39–81	15–105
				132–160	37–42
UTG-631	0.787	7.1	60	88–148	25–100
				311–346	40–50
UBG-425	0.635	7.1	45	98.9–148	20–60
				411	45
UTG-622	0.559	7.1	60	115–192	15–90
				435–480	40–50
UTG-618	0.457	7.1	60	148–198	15–42
				520–577	45–55
UTG-614	0.355	7.1	60	182–249	15–47
				750	51
UTG-610	0.254	7.1	60	291	29
				736	31

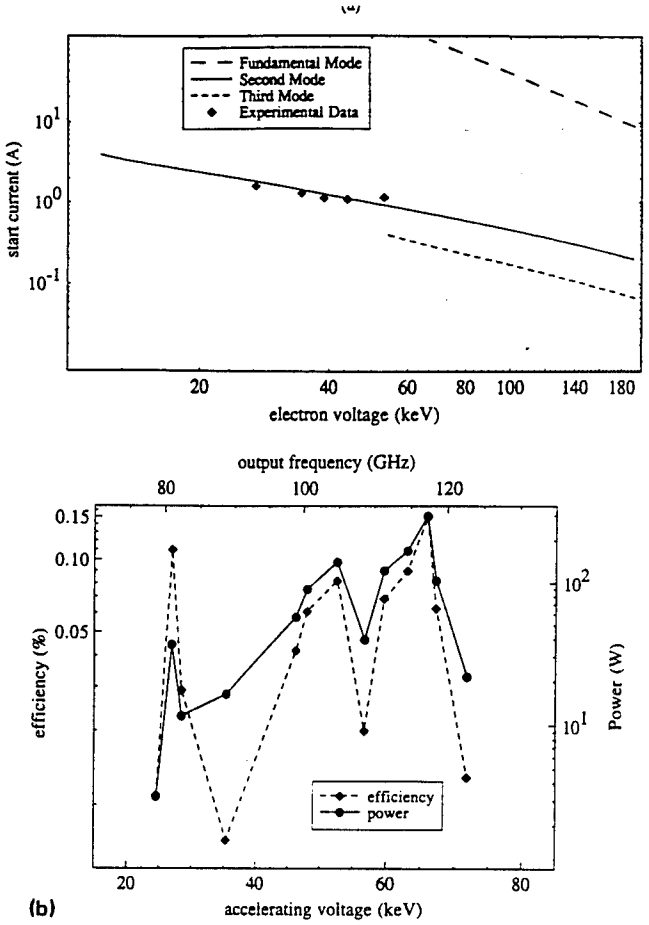

FIG. 4. The operating parameters for UTG-631 are shown in two plots. (a) The theoretical start current (lines) are plotted together with data (diamonds) vs electron beam energy. (b) Experimental power (circles) and efficiency (triangles) are plotted vs beam energy. Here, the lines merely connect the experimental points.

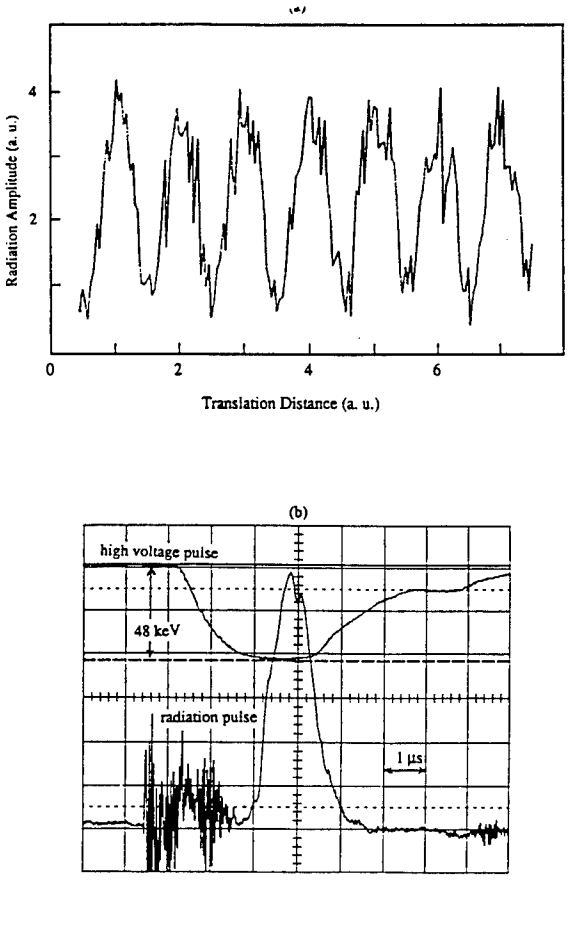

FIG. 5. Raw experimental data of GCO radiation at 346 GHz in two forms. (a) A Michelson interferogram is used to determine the output frequency via the period of the amplitude variations. (b) An oscilloscope trace of the radiation output signal is shown with its corresponding 48 keV high voltage pulse.

operation have been successful. Results are compiled in Table I. In all cases, two modes of operation are seen. It can be seen that the LFM occurs as a result of Smith–Purcell radiation emitted at a backward (with respect to beam propagation direction) angle while the HFM corresponds to a synchronous coupling on a second space harmonic component. This results in forward angle emission. Future experiments will revolve around the utilization of novel optical schemes to enhance feedback for specific angular components. Operation at 100 μm wavelengths with modest (less than 100 keV) electron beam energies is theoretically possible. A Michelson interferogram indicating stable HFM operation at 346 GHz is shown in Fig. 5 along with an example of the output radiation signal/high voltage pulse.

The power at the detector has been measured as a function of the accelerating voltage. The LFM power as a function of beam voltage (output frequency) for UTG-631 is shown in Fig. 4. Corresponding values of the efficiency are also shown. Fluctuations in power over the spectral range have been noted for all gratings. This may be due to the change in the cavity Q with respect to the operating wavelength. Power levels of the two modes were measured to be hundreds of watts and watts, respectively. Configuring the resonator optics to facilitate feedback of the forward-angle radiative component should result in increased power levels of the HFM signal. It is expected that an optimized experiment will result in electronic efficiencies characteristic of traveling-wave devices (i.e., 10%–20%).

In conclusion, it is seen that GCO devices possess the potential to serve as tunable radiation sources at wavelengths shorter than 1 mm. The simple, rugged, and compact design of the GCO make it an attractive alternative to other sources currently operating in this area. Future experiments will seek to exploit the HFM operation in order to achieve device operation in the 100 μm region.

The support of Vermont Photonics, Inc. and USARO Contract No. DAAL03 91-G-0189 is gratefully acknowledged.

[1] S. J. Smith and E. M. Purcell, Phys. Rev. **92**, 1069 (1953).
[2] E. S. Rusin and G. D. Bogomolov, JETP Lett. **4**, 160 (1966).
[3] K. Mizuno, S. Ono, and Y. Shibata, *Proceedings of the Symposium on Submillimeter Waves* (Polytechnic, New York, 1971), p. 115.
[4] W. W. Salisbury, J. Opt. Soc. Am. **60**, 1279 (1970).
[5] I. Shih, W. W. Salisbury, D. L. Masters, and D. B. Chang, J. Opt. Soc. Am. B **7**, 345 (1990).
[6] D. E. Wortman, R. P. Leavitt, H. Dropkin, and C. A. Morrison, Phys. Rev. A **24**, 1150 (1981).
[7] E. M. Marshall, P. M. Phillips, and J. E. Walsh, IEEE Trans. Plasma Sci. **PS-16**, 199 (1988).

First Observation of Smith Purcell Radiation from Relativistic Electrons. G. DOUCAS, J.H. MULVEY and M. OMORI, Oxford University; J. WALSH, Dartmouth College, USA; M. KIMMITT, Essex University - The Oxford 10 MV Van der Graaff has been converted to accelerate electrons. A pulsed beam of 3.6 MeV, peak current about 0.1 A over 5 miro s., was used to investigate spontaneous emission by the Smith Purcell mechanism using gratings of 7cm length and periods of 450, 760, and 1000 microns. The radiation was analysed with a Czerny-Turner spectrometer and a liquid helium cooled indium-antimonide detector. Results will be presented on the emission in the far infra-red at angles between 60 and 130 degrees to the electron beam direction, and wavelengths from 350 to 1650 microns.

Apr. 1992

Submitted by: J.H. Mulvey
Oxford University
Nuclear Physics Laboratory
Keble Road
Oxford OX1 3RH
UK

Classification Number: A08

Desired presentation option: (circle) Oral Poster No choice

Mail to: EPAC Scientific Secretariat
c/o Mrs. Ch. Petit-Jean-Genaz
CERN - AC
CH - 1211 Geneva 23

3. List of All Publications and Technical Reports

Technical Reports:

Progress Report, July 1993.
Progress Report, October 1992.
Progress Report, March 1992.

Publications and Presentations:

In addition to the publications listed as Technical Appendices in Section 2 of this Report, the following conference presentations and publications were completed with support of Army Research Office Contract DAAL03-91-G-0189:

1. *Far-Infrared Smith-Purcell Experiment: Measurement of Radiated Power,* Nucl. Instruments & Methods A **331**, 609 (1993).

2. *Observations of Relativistic Electron-Beam-Generated Smith-Purcell Radiation,* Bull.Am.Phys.Soc. **37,** 934 (1992).

3. *Smith-Purcell Radiation at Submillimeter and Far-Infrared Wavelengths,* Proceedings of the 17th International Conference on Infrared and Millimeter Waves, Pasadena, Ca., December 1992.

4. *Radio-Frequency-Injector-Driven Cherenkov Free-Electron Laser,* Nucl. Instruments & Methods A **318,** 772 (1992).

5. *Smith-Purcell Radiation from a Relativistic Electron-Beam-Driven Grating,* Bull.Am.Phys.Soc. **37**(2), 1761 (1992).

6. *Grating-Coupled Oscillator Experiments at Submillimeter/FIR Wavelengths,* 16th International Conference on Infrared and Millimeter Waves, August 1991.

7. *Submillimeter-Wavelength Radiation from a Grating-Coupled Source,* Bull.Am.Phys.Soc. **36,** 2403 (1991).

8. *Diffraction-Grating and Dielectric-Film-Coupled Free-Electron Lasers,* 13th International Free-Electron Laser Conference, Santa Fe, August 1991.

4. List of All Participating Scientific Personnel

1. John E. Walsh, Principal Investigator.

2. Maurice F. Kimmitt, Visiting Scientist.

3. Richard Cook, Research Engineer.

4. Edwin J. Price, Ph.D. April, 1991.

5. Emily E. Fisch, Ph.D. September, 1991.

6. Joseph H. Killoran, Ph.D. October, 1993.

7. Fred L. Hacker, Ph.D. June ,1994.

8. Michael Goldstein, Ph.D. October, 1994.

5. Bibliography

Edwin J. Price, Ph.D. Thesis, April 1991, *Operation of a Smith-Purcell Free-Electron Laser at Submillimeter Wavelengths.*

Emily E. Fisch, Ph.D. Thesis, September 1991, *The Sapphire Cherenkov Laser.*

Garret Piech, Senior Honors Thesis, June 1992,*Investigation of an Open Fabry-Perot Cavity.*

Stephen G. Yeager, Senior Honors Thesis, June 1993, *A Dipole Model of Smith-Purcell Radiation.*

Joseph H. Killoran, Ph.D. Thesis, October 1993, *Investigations of a Smith-Purcell Free-Electron Laser: The Grating Seen as a Diffractive Element.*

E. Kirk Miller, Senior Honors Thesis, June 1994, *Investigation of the Infrared Radiation from a Short-arc, High-pressure Mercury Discharge Lamp.*

Fred L. Hacker, Ph.D. Thesis, June 1994, *Mode-Locking in a Grating-Coupled Oscillator.*

Michael Goldstein, Ph.D. Thesis, October 1994, *A Far-Infrared Smith-Purcell Micro-Radiator.*

One set of theses is included with this report. Copies have also been furnished to the ARO Library. Further copies may be requested from the Dartmouth College Physics Department, Plasma Physics Laboratory, 6127 Wilder Laboratory, Hanover, N.H. 03755-3528.